Edited by Z. Bažant


*Chapter 13*

# *Fracture in Concrete and Reinforced Concrete*

*Z. P. Bažant*

## 13.1 INTRODUCTION

Although cracking represents a salient feature of the behaviour of concrete structures, not only under ultimate loads but also at service states, fracture mechanics has not been used in practical analysis of structures. Structural engineers had a good reason; the linear fracture mechanics was found to be inapplicable to typical concrete structures, and the premises of ductile fracture mechanics did not match material behaviour. However, in various recent investigations, particularly those at the Technical University of Lund, Northwestern University, and Politecnico di Milano, it has been shown that fracture mechanics can be applied to concrete structures provided that one takes into account the effect of a large micro-cracking zone or fracture process zone that always exists at the fracture front.

The objective of the present paper is to review the results of the investigations at Northwestern University, many of them carried out under a cooperative agreement with Politecnico di Milano (as part of the Italy–US Science Cooperation Program), and also to present some new results on a continuum model for strain-softening and on R-curve analysis. It is not possible to include a comprehensive review of all the work on fracture of concrete; other work may be consulted for that (Wittmann, 1983; Mindess, 1983; Ingraffea, 1984; Shah, 1984; ASCE, 1982; Bažant, 1984).

## 13.2 BLUNT CRACK BAND MODEL

The simplest way to model cracking in a finite element program is to assume that the cracks are continuously distributed over the area of the finite element and manifest themselves by a reduction of the elastic modulus in the direction normal to the cracks. Complete cracking corresponds to a reduction of the elastic modulus to zero. In this description, introduced by Rashid (1968), the crack band front obviously cannot be narrower than the width of the frontal finite element.

It has not been generally recognized, however, that, normally, the width of the

crack band front also cannot be wider than a single element. Of course, one could enforce the crack front to be of a multiple-element width, however, that would not be justified mechanically since localization of strain into a single-element width generally leads to a release of elastic energy. There is a further reason why a multiple-element width at the crack band front is not a correct model; if we make the loading step sufficiently small, then only one element cracks during the loading step, and this relieves the stresses in the finite element that is on the side of the element that has just cracked, thus preventing an increase of the crack front width, except if a uniform strain distribution is enforced by heavy reinforcement. Even if two finite elements at the crack front had exactly the same stress values, it would be unrealistic to assume that they both crack simultaneously since the statistical scatter of material properties will always cause one of these elements to crack before the other does. Thus, one may adopt the blunt crack band model with a single-element wide front as a realistic and numerically convenient model for cracking in concrete (Bažant, 1982; Bažant and Cedolin, 1979, 1980, 1983; Bažant and Oh, 1983a; Cedolin and Bažant, 1980; Bažant *et al.*, 1983b). A similar approach can be applied to rock (Bažant, 1982; Bažant and Oh, 1982).

Regardless of whether the zone of micro-cracking at the fracture front in

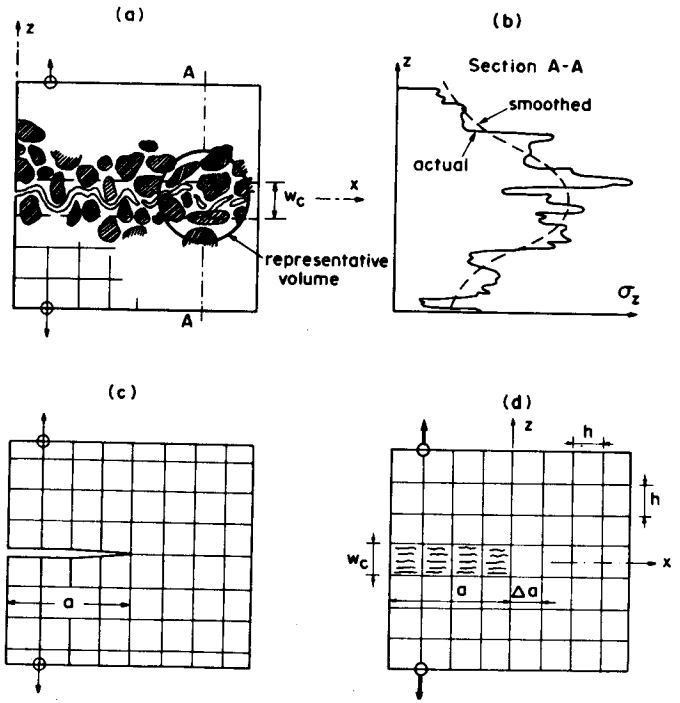


Figure 13.1 Heterogeneous microstructure, random scatter of stresses, and finite element models (after Bažant and Oh, 1982)



concrete is very wide or not, two elementary justifications may be offered for the blunt crack band model. One of them is the heterogeneity of the material. We treat the material as a smoothed, homogeneous continuum in the macroscopic sense. In this treatment, the macroscopic stresses and strains represent the averages of the actual (microscopic) stresses and strains over a certain so-called representative volume of the material whose size must be at least several times the maximum aggregate size (Figure 13.1). Obviously, the rapid and scattered variation of stresses and strains over smaller distances cannot be described by a continuum approach. Therefore, using finite elements of sizes less than several times the aggregate size would not allow any improvement in the description of the actual stress and strain fields within concrete. Even if one wishes to treat a continuous sharp crack in concrete, the blunt crack band model does not represent the reality any worse than a sharp inter-element crack model because the actual crack path is not straight but highly tortuous.

As another justification of the blunt crack band model for describing sharp fractures in concrete, one may cite the recently documented fact that a sharp inter-element crack and a blunt crack band of single-element width yield approximately the same results if the mesh is not too crude (roughly when there are at least fifteen finite elements in a square mesh across the cross-section). Both models give energy release rates that differ not more than a few per cent from the exact elasticity solution. To illustrate it, Figure 13.2 exhibits some of the numerical results from Bažant and Cedolin (1979). In these calculations, the normal stress in the direction perpendicular to the cracks was assumed to drop suddenly to zero when the energy criterion for crack band propagation became satisfied. The finite element mesh in Figure 13.2 covers a cut-out of an infinite elastic medium loaded at infinity by uniform normal stress $\bar{\sigma}$ perpendicular to a line crack of length $2a$. The nodal loads applied at the mesh boundary are calculated as the resultants of the exact stresses in the infinite medium, based on Westergaard's exact solution which is shown as the solid curve. The data points in Figure 13.2 show numerical results for the square mesh shown (mesh A), as well as for finer meshes B and C (not shown) for which the element size was 1/2 and 3/8 of the element size shown, respectively. A similar equivalence of results for the sharp inter-element crack and the blunt crack band can be demonstrated when the stress is considered to drop gradually rather than suddenly to zero (Bažant and Oh, 1983a).

Aside from the foregoing justifications, the blunt crack band model appears to be more convenient for finite element analysis. When a sharp inter-element crack gets extended through a certain node, the node must be split into two nodes. This increases the total number of nodes and changes the topological connectivity of the mesh. Unless the nodes are renumbered, the band structure of the structural stiffness matrix is lost. Moreover, if the direction in which an inter-element crack should extend is not known in advance, one needs to make trial calculations for various possible locations of the node ahead of the crack front through which the

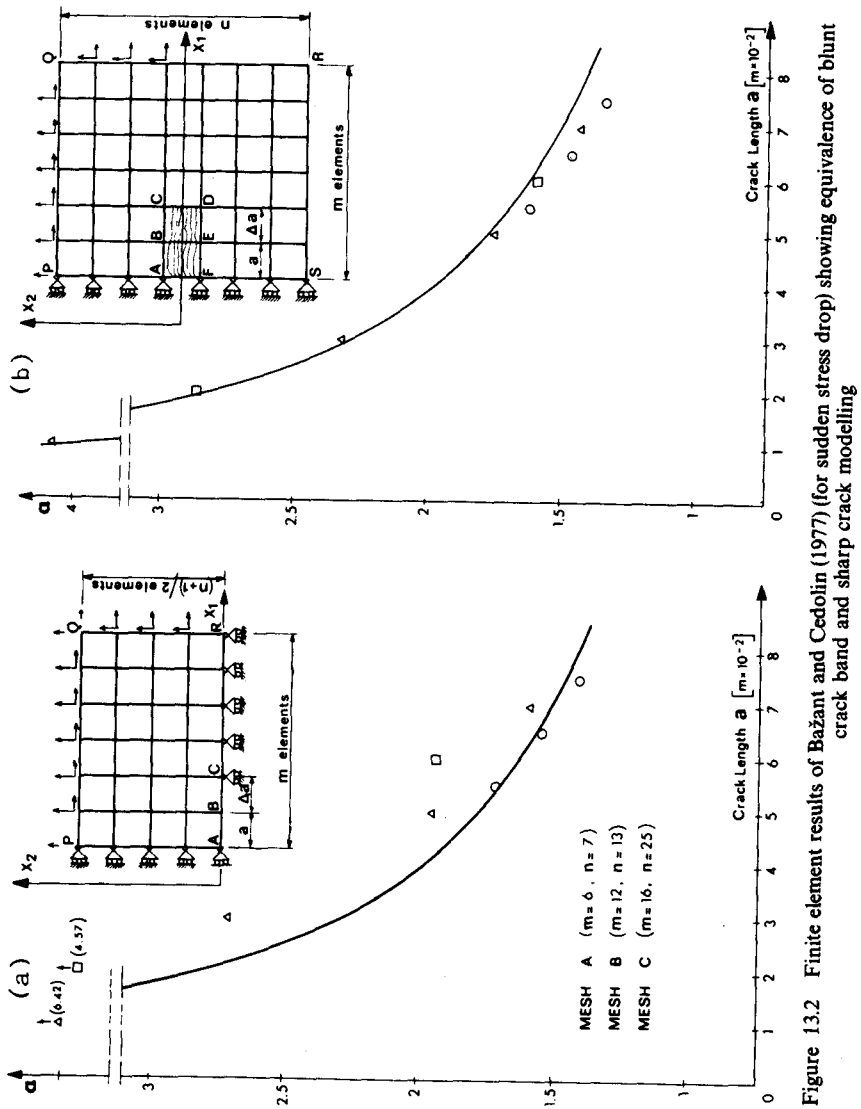


Figure 13.2 Finite element results of Bažant and Cedolin (1977) (for sudden stress drop) showing equivalence of blunt crack band and sharp crack modelling



crack should pass, in order to determine the correct direction of crack propagation. On the other hand, in the blunt crack band model, a fracture propagating in any direction through the mesh can be modelled as a zigzag crack band with any direction of the cracks relative to mesh lines. All that needs to be done to model an oblique crack direction is to reduce the elastic stiffness in the direction normal to the cracks.

Recently, various attempts to observe the distribution of micro-cracks ahead of the fracture front in concrete have been made (Mindess and Diamond, 1980; Cedolin *et al.*, 1983a, 1983b). From strain measurements by Moiré interferometry (Cedolin *et al.*, 1983a, 1983b), it appears that the width of the micro-crack zone at the fracture front is about one aggregate size. Within this width, there is a crack concentration. However, the line along which the densest micro-cracks are scattered is not straight but rather tortuous (Figure 13.1), which would not be modelled by a straight inter-element crack any better than by a crack band. Correlation of the crack band model to such microscopic observation is, of course, difficult since the micro-crack density varies while in the crack band it is assumed to be uniform. The question then is at which micro-crack size to draw the distinction. Thus, the width of the microscopically observed crack band front depends on the definition of the width of the micro-cracks that are counted within the crack band.

One significant difference from ductile fracture of metals consists in the size of the fracture process zone, defined as the zone in which the material undergoes strain-softening, i.e. the maximum principal stress decreases at increasing strain. This zone is large for concrete but relatively small for metals, even in the case of ductile fracture. In the latter case, there is a large yielding zone, but the material does not undergo strain-softening in this zone (Figure 13.3).

The stress–strain relation with strain-softening for the fracture process zone may be replaced by a strain–displacement relation if the displacement represents the integrated value of the strains across the width of the crack front. In this sense, the present blunt crack band model is equivalent to the previous line crack models with softening stress–displacement relations, introduced by Barenblatt, 1959; Dugdale, 1960; Kfouri and Miller, 1974; Kfouri and Rice, 1977; Knauss,

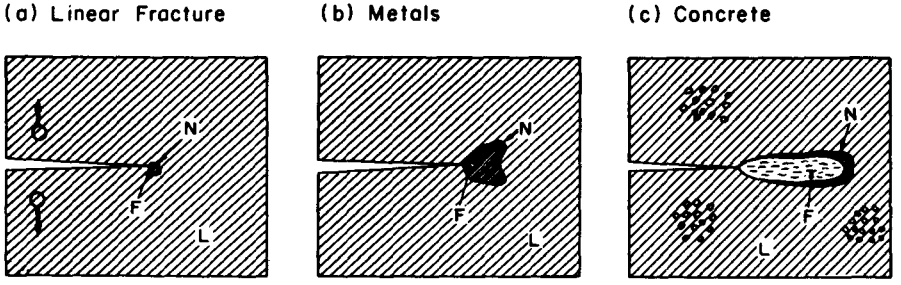


Figure 13.3 Nonlinear zone N and fracture process zone F for various materials

1974; Wnuk, 1974; Hillerborg *et al.*, 1976. For concrete this approach was pioneered by Hillerborg, Modéer, and Petersson (1976) and Petersson (1980) in their model of a fictitious sharp inter-element crack.

Let us now outline one possible form of the softening stress–strain relation for the fracture process zone. Let the virgin crack-free material be described by the elastic stress–strain relation

$$\boldsymbol{\varepsilon} = \mathbf{C}\boldsymbol{\sigma} \tag{13.1}$$

Here, $\boldsymbol{\sigma}$, $\boldsymbol{\varepsilon}$ are the column matrices of the cartesian normal components of strain and stress, in cartesian coordinates $x_1 = x$, $x_2 = y$, and $x_3 = z$. $\mathbf{C}$ is a $3 \times 3$ square compliance elastic matrix of the virgin material, with components $C_{11}$, $C_{12}, \ldots, C_{33}$. For the sake of simplicity, we may now assume that all micro-cracks spread over the finite element are normal to axis $z$. Appearance of such cracks has no effect on the lateral strains $\varepsilon_x$ and $\varepsilon_y$, and the only effect is an increase in the averaged normal strain $\varepsilon_z$ in the direction perpendicular to the cracks. This may be described by cracking parameter $\mu$ introduced only in one diagonal term of the compliance matrix (Bažant, 1982; Bažant and Oh, 1983a)

$$\mathbf{C}(\mu) = \begin{bmatrix} C_{11} & C_{12} & C_{13} \\ & C_{22} & C_{23} \\ & & C_{33}\mu^{-1} \end{bmatrix} \tag{13.2}$$

The cracking parameter $\mu$ is 1 for the initial crack-free state, and approaches zero for the final fully cracked state. It has been shown (Bažant and Oh, 1983a), that the limit of the inverse of the compliance matrix $C(\mu)$ as $\mu \to 0$ is, exactly, the well-known stiffness matrix for a fully cracked elastic material, $\mathbf{D}^{fr}$. This matrix is identical to the elastic stiffness matrix for the plane state of stress, which exists in the material between the cracks.

The cracking parameter may be calibrated so as to yield the desired tensile stress–strain relation with strain-softening $\sigma_z = EF(\varepsilon_z)$, in which $E = 1/C_{33} =$ Young's modulus. Then one has $\mu = F(\varepsilon_z)/\varepsilon_z$. Function $F(\varepsilon_z)$ may be given as a bilinear stress–strain diagram (Figure 13.4), characterized by tensile strength $f_t'$, softening modulus $E_t$ (negative), and limit strain $\varepsilon_0$ for which full cracks are formed. For computer analysis, the foregoing stress–strain relation is differentiated to obtain an incremental form to be used in a program with step-by-step loading.

The strength limit, $f_t'$, needs adjustment to take into account the effect of multiaxial stress state. In particular, the tensile strength limit is decreased due to normal compressive stresses $\sigma_x$ and $\sigma_y$ parallel to the crack plane. Correction may be done according to the well-known biaxial failure envelope for concrete (Bažant and Oh, 1983a) (Figure 13.4(d)).

The use of cracking parameter $\mu$ resembles the so-called continuous damage mechanics, in which damage is characterized by parameter $\omega$ which corresponds



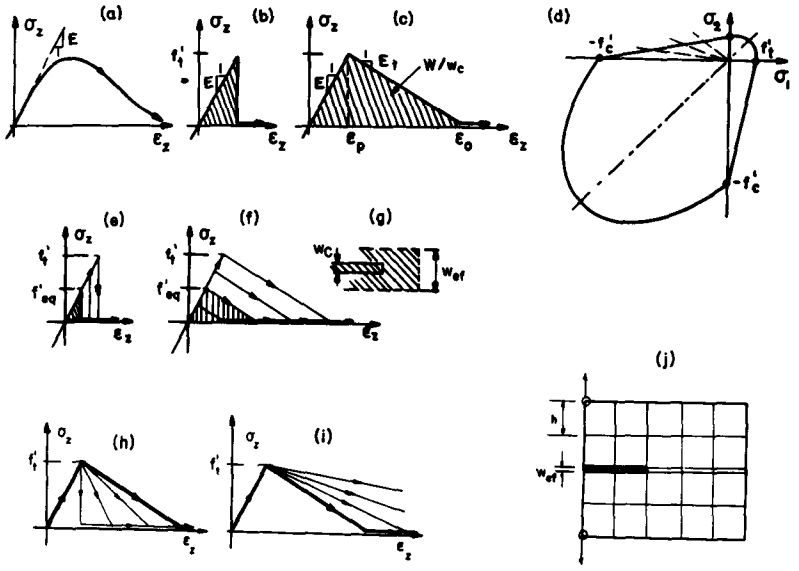


Figure 13.4 Tensile stress–strain diagrams assumed for fracture analysis

to $1 - \mu$. There is, however, a fundamental difference in that the damage due to micro-cracking is considered to be inseparable from a zone of a certain characteristic width that is a material property, as we will explain later.

The energy consumed by crack formation per unit area of the crack plane, i.e.

$$G_f = W_f w_c, \quad W_f = \int_0^{\varepsilon_0} \sigma_z \, d\varepsilon_z \tag{13.3}$$

represents the fracture energy; $w_c$ = width of the crack band front (fracture process zone), and $W_f$ = work of maximum principal tensile stress per unit volume = area under the uniaxial tensile stress–strain curve (Figure 13.4).

The magnitude of $w_c$ is obviously an important factor. If the stress–strain relation, including its strain-softening range, is considered to be a material property, which seems logical, then the larger is $w_c$ the larger is the fracture energy $G_f$. It has been previously demonstrated (Bažant and Cedolin, 1979, 1980), however, that finite element calculations yield results independent of the choice of the element size (except for a negligible numerical error converging to zero) only if the fracture energy $G_f$ is considered as a material constant. Equation (13.3) then indicates that the width $w_c$ of the crack band front must also be a material constant, to be determined by tests. Indeed, if the value of $w_c$ is changed without adjusting the strength limit $f_t'$ or the strain-softening modulus $E_t$, the predicted values of loads needed for further crack propagation may change drastically (Bažant and Cedolin, 1979, 1980). For the bilinear tensile stress–strain relation

(Figure 13.4), energy balance requires that

$$W_f = \tfrac{1}{2}(C_{33} - C^t_{33}) f'^2_t w_c = \tfrac{1}{2} f'_t \varepsilon_0 w_c$$

or

$$w_c = \frac{2G_f}{f'^2_t} \frac{1}{C_{33} - C^t_{33}} \tag{13.4}$$

in which $C^t_{33} = 1/E_t$ (negative) and $C_{33} = 1/E$. Thus, the effective width of the crack band front may be determined by measuring the tensile strength, the fracture energy, and the softening modulus $E_t$.

Note that Equation (13.4) is similar to the well-known Irwin's expression for the size of the yielding zone. It should be also noted that determination of $w_c$ from mechanical measurements depends on the knowledge of the strain-softening slope $E_t$. If this slope is changed, a different value of $w_c$ is obtained, and fracture test data may still be fitted equally well, within a certain range of $w_c$. In fitting test data for concrete fracture from the literature, it has been noted that good fits could be obtained for $w_c$ ranging from $2d_a$ to $4d_a$ where $d_a$ is the maximum aggregate size. The front width

$$w_c = 3d_a \tag{13.5}$$

was nearly optimum, and at the same time was consistent with the softening modulus $E_t$ as observed in the direct tension tests of Evans and Marathe (1968), Heilmann *et al.*, (1969), Rüsch and Hilsdorf (1963), Petersson (1981), and Reinhardt and Cornelissen (1984).

Most of the important test data from the literature (Brown, 1972; Carpinteri, 1980–1981; Entov and Yagust, 1975; Gjørv *et al.*, 1977; Huang, 1981; Kaplan, 1961; Kesler *et al.*, 1971; Mindess *et al.*, 1977; Naus, 1971; Shah and McGarry, 1971; Shah, 1984; Sok *et al.*, 1979; Schwartz *et al.*, 1981; Walsh, 1972; Wecharatana and Shah, 1980; Petersson, 1981), have been fitted with good success using the present nonlinear fracture model (Bažant and Oh, 1983a). Some of the fits obtained in Bažant and Oh (1983a) by finite element analysis using square meshes are shown in Figures, 13.5 and 13.6, in which $P_{max}$, representing the maximum measured load, is plotted as a function of either the crack length (flaw depth) or the specimen size. The optimum fits obtainable with linear elastic fracture mechanics are shown for comparison in these figures as the dashed lines. In calculating these results, the loading point was displaced in small steps and the reaction, representing load $P$, was evaluated at each loading step by finite elements. The same bilinear stress–strain relation (Equation (2)) was assumed to hold for all elements.

Note that the crack band fracture theory models well not only the test results for notched fracture specimens, but also the results for unnotched beams, in which the nominal bending stress at failure decreases as the beam depth increases (Figure 13.6h). This phenomenon is due to the fact that the large fracture process zone (strain-softening zone) cannot be fully accommodated in a small



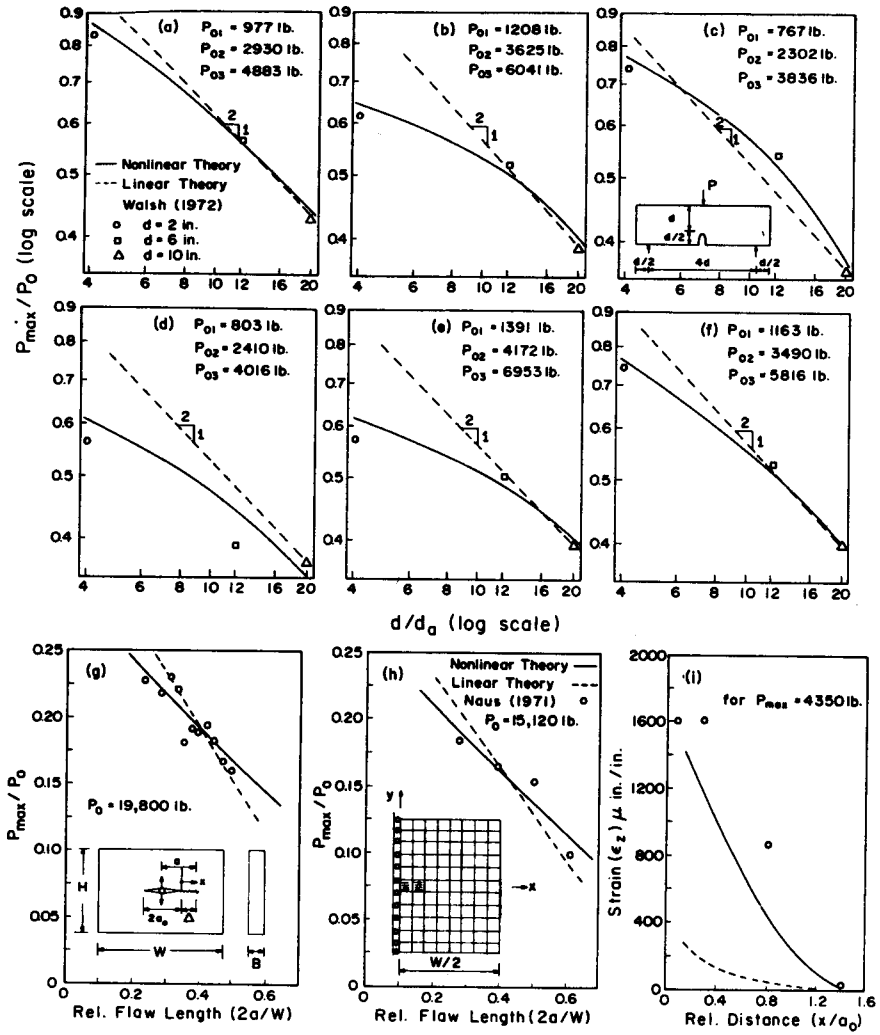


Figure 13.5 Results of crack band analysis compared with maximum load test data from the literature (after Bažant and Oh, 1983)

beam. The same phenomenon was previously modelled as a statistical size effect; however, explanation in terms of fracture mechanics, previously proposed by Hillerborg, appears to be more correct.

For metals, deviations from linear fracture mechanics have been described by the so-called R-curves (resistance curves), which represent the variation of apparent fracture energy as a function of the crack extension from a notch. Based on an idea of Irwin and Krafft *et al.* (1961), the *R*-curve may be considered for most situations as a fixed material property, although in reality this can be

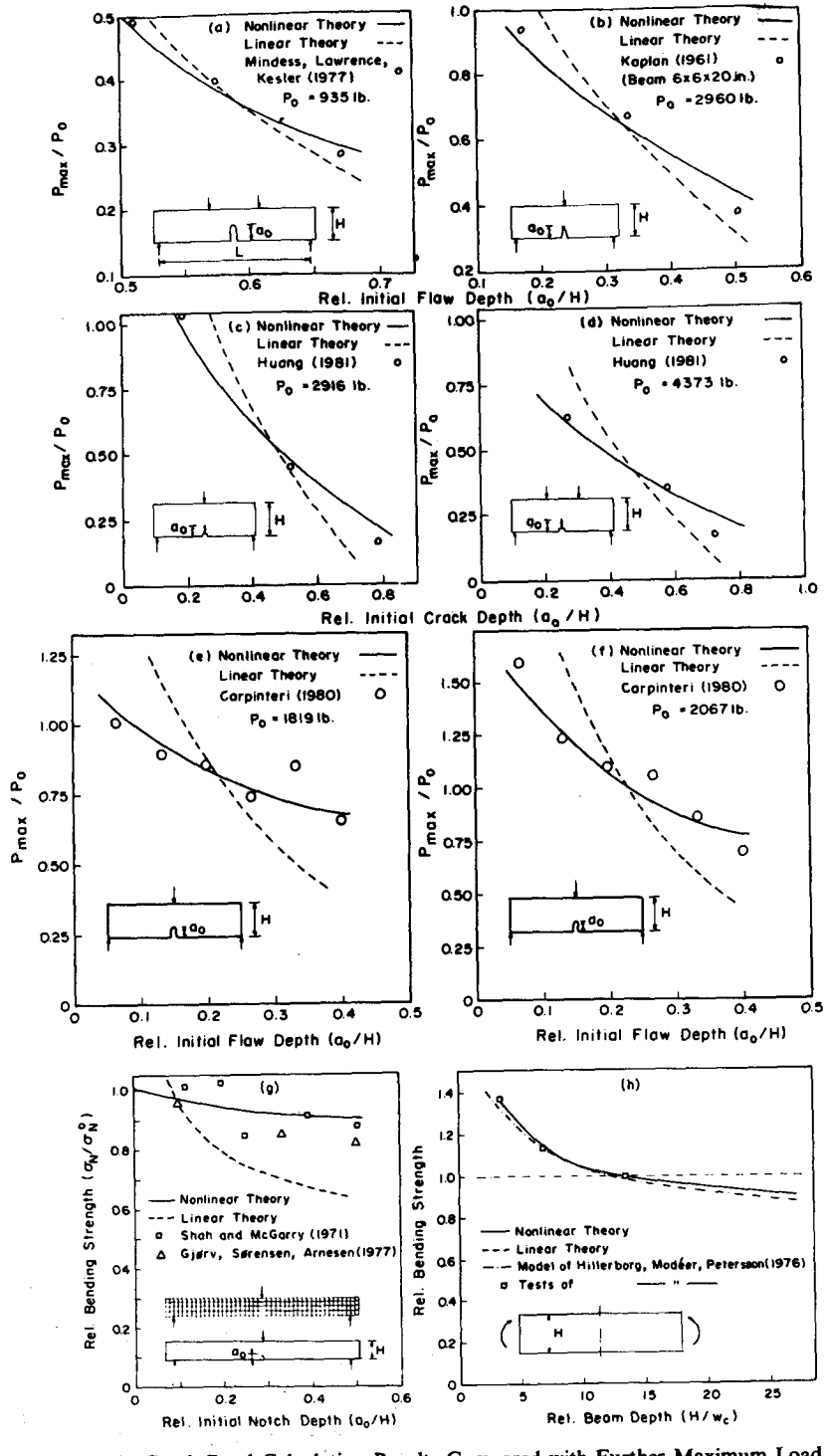


Figure 13.6 Crack Band Calculation Results Compared with Further Maximum Load Test Data From the Literature (after Bažant and Oh, 1983)



exactly true only asymptotically, for infinitely small crack extensions from a notch (for longer extensions, the R-curve should, in theory, also depend on the boundary geometry, location of the loads, crack path, etc.). It is noteworthy that the present theory achieves a good fit of test data without introducing any variation of fracture energy $G_f$, i.e. $G_f$ is a constant. In fact, the present theory

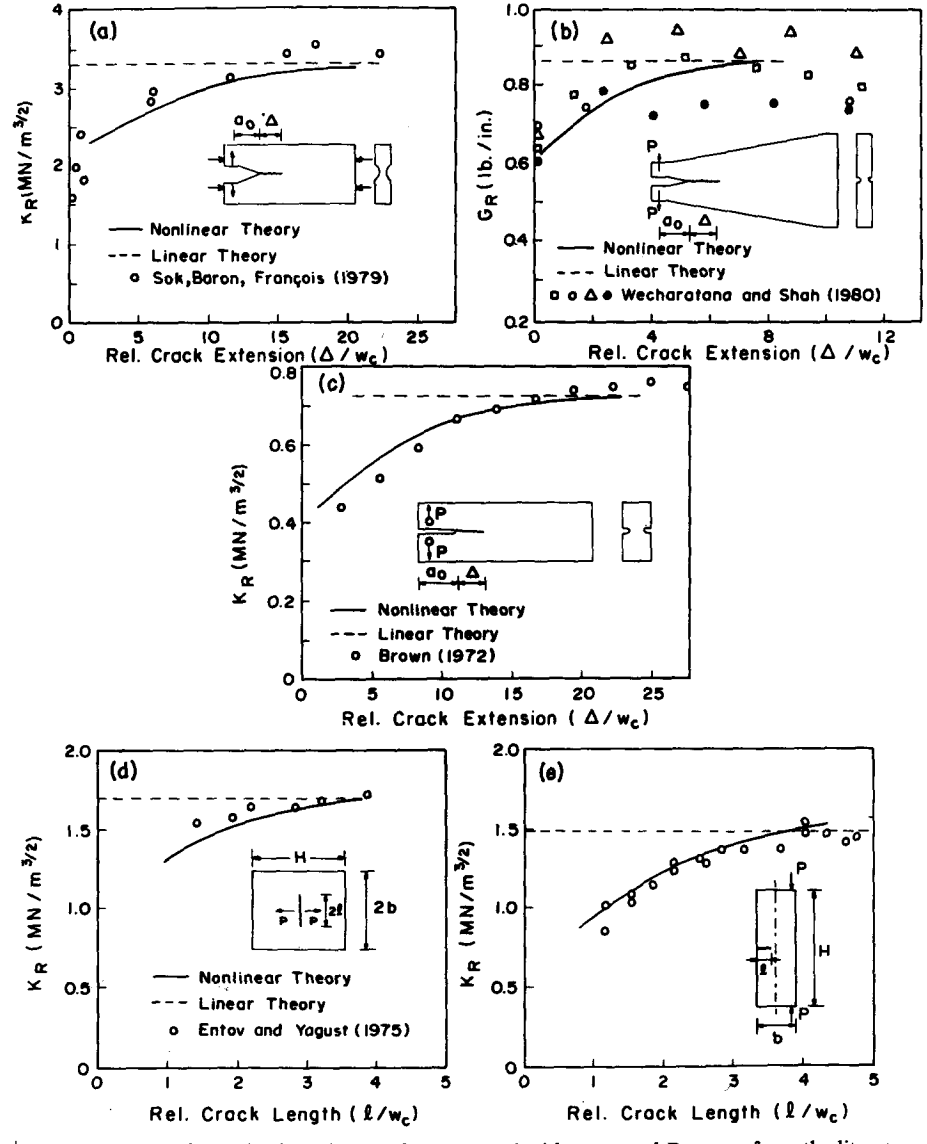


Figure 13.7 Crack band calculation results compared with measured R-curves from the literature (after Bažant and Oh, 1983)

allows calculating the R-curves. For this purpose one needs to evaluate the work of the nodal forces acting at the crack front element during a small crack band extension. In this manner, the R-curves have been calculated using the same fracture parameters as in the previous fitting of maximum load data. These calculations have led to good fits of R-curve data reported in the literature (Bažant and Oh, 1983a); see Figure 13.7, using test data from Brown, 1972; Entov and Yagust, 1975; Sok *et al.*, 1979; Wecharatana and Shah, 1980. For the details of analysis, see Bažant and Oh, 1983a. It is worth noting that the present theory has been also used with equal success to fit the test data for various rocks (Bažant, 1982; Bažant and Oh, 1982).

Statistical analysis of the test data available in the literature revealed that the crack band theory allows a great reduction of the coefficient of variation $\omega_0$ of the deviations of test data from the theory, as compared to previous theories. In the case of maximum load data, $\omega_0 = 0.066$ for the present theory, while for the best fits with linear elastic fracture mechanics, $\omega_0 = 0.267$. For the strength criterion, $\omega_0 = 0.650$ (see Bažant and Oh, 1983a). In the case of R-curve data, the present crack band theory yields for the deviations of test data from the theory the standard deviation $s = 0.083$, while linear fracture mechanics with constant fracture energy yields $s = 0.317$; see Bažant and Oh (1983a). These are significant improvements in the error statistics, and the accuracy of the present crack band theory is seen to be sufficient for practical purposes.

The analysis of test data from the literature also has resulted into an approximate empirical formula for the prediction of fracture energy on the basis of tensile strength $f_t'$, maximum aggregate size $d_a$, and Young's modulus $E$;

$$\tilde{G}_f \simeq 0.0214(f_t' + 127)f_t'^2 d_a/E \tag{13.6}$$

in which $f_t'$ must be in psi (psi = 6895 Pa), and $\tilde{G}_f$ is in lb/in. Exploiting the relation $G_f \simeq 3d_a f_t'^2(E^{-1} - E_t^{-1})/2$, one can further obtain a prediction formula for the softening modulus

$$E_t \simeq \frac{-69.9E}{f_t' + 56.7} \tag{13.7}$$

## 13.3 APPLICATION IN FINITE ELEMENT PROGRAMS

Finite elements of size $h = w_c = 3d_a$ may be too small for many practical applications. However, we cannot simply increase the element size because according to Equation (13.3) the energy consumed by fracture would increase proportionally with $h$, other parameters remaining unchanged. Obviously, in order to maintain the same energy consumption by fracture, the area under the tensile stress–strain diagram must be changed in inverse proportion to the element width $h$. This may be done most conveniently by adjusting the strength



limit from the actual strength $f_t'$ to a certain equivalent tensile strength $f_{eq}'$; Figure 13.4(f). If we use the bilinear stress–strain diagram and keep the softening modulus $E_t$ constant, we obtain the following expression for the equivalent strength in a square mesh in which the fracture propagates parallel to the mesh line;

$$f_{eq}' = c_f\left(1 + \frac{E}{-E_t}\right)^{-1/2}\left(\frac{2G_f E'}{hr_f}\right)^{1/2} \tag{13.8}$$

in which $c_f$ is a calibration factor close to 1, depending on the type of finite element, and $r_f$ is a correction for the compressive normal stress $\sigma_3$ parallel to the crack plane; $r_f \simeq 1 - \nu'\sigma_3/\sigma_1$ where $\nu' = \nu/(1-\nu)$, $\nu$ = Poisson ratio. We see from Equation (13.8) that the tensile strength limit must be reduced in inverse proportion to the square root of element size $h$.

Alternatively, one may make the declining slope steeper while keeping the same peak stress (Figure 13.4(h)). The slope is again chosen so as to ensure correct energy dissipation (Bažant and Oh, 1983a). The maximum element size that can be used with this approach corresponds to the vertical stress drop (Figure 13.4(e), (h)), and if still larger elements need to be used, then the strength limit needs to be reduced using a vertical stress drop (Figure 13.4(e)).

If the fracture path is known, one may also enlarge the finite elements outside the crack band while keeping the elements of the crack band at the correct width $w_c$ (Figure 13.4(j)) and using the actual stress–strain diagram. As still another alternative, a transition to the line crack model of Hillerborg *et al.*, may be obtained by reducing the band width below $w_c$, in which case the declining slope of the stress–strain diagram must be made milder (Figure 13.4(i)) so as to preserve the correct energy dissipation.

If the tensile strength limit (or the declining slope) is not changed when the element size changes, fracture analysis is unobjective in that the results may strongly depend on the analyst's choice of the element size. The first example of this was presented in Bažant and Cedolin (1983a) in which a rectangular panel, either plane or reinforced, was analysed for propagation of a symmetric central crack band. It was demonstrated that by changing the element size four times, the calculated value of the load needed for further crack band propagation changed by a factor of 2 (i.e. by 100 per cent). This implies a gross error in the prediction of energy absorption in the structure.

It should be realized, however, that keeping the strength limit and the declining slope the same regardless of the element size does not always lead to wrong results. In fact, for many situations finite element analyses with a constant tensile strength yielded good results, in agreement with tests. The reason why this happens is that many structures are fracture-insensitive, i.e. their failure depends primarily on other phenomena such as plastic yielding of steel rather than on

cracking of concrete. The flexural failure of reinforced beams is a good example. To decide whether the problem is fracture-insensitive, the analyst needs to run the finite element calculations twice: once with the actual tensile strength $f'_t$, and once with a zero tensile strength. If the results do not differ significantly, one may forget about fracture mechanics.

For structures much larger than the aggregate size, the size of the fracture process zone may become negligible compared to the cross-section dimensions (this is true, for example, for gravity dams). If the finite elements are not very small, a small fracture process zone can be obtained by considering a vertical stress drop (Figure 13.4(b), (e)) instead of gradual strain-softening. A small fracture process zone is a prerequisite for the validity of linear elastic fracture mechanics, and indeed it is found (Bažant, 1982; Bažant and Oh, 1983a) that the use of a sudden stress drop after the tensile strength limit has been reached leads to results that are very close to the exact solutions of linear elastic fracture mechanics (Bažant and Cedolin, 1979). The energy release rates obtained with the present crack band model are just as close to the exact solution as those obtained with the sharp inter-element crack model (Bažant, 1982).

When a vertical stress drop is assumed, the energy criterion of fracture mechanics can be more closely approximated by a direct calculation of the energy release due to crack band extension, rather than by the use of a certain tensile stress–strain diagram with equivalent strength. A formula for the change in potential energy due to crack band extension was given in Bažant (1982) and Bažant and Oh (1983a). In this formula, one calculates the work of the nodal forces acting upon the frontal finite element during the fracture formation. One must also consider the differences between the initial and final strain energy within the cracked frontal finite element, as well as the work of distributed forces transmitted from reinforcement to concrete.

Instead of directly calculating the work of nodal forces on the frontal finite element, one may also obtain the exact energy release through the use of the J-integral. This method of analysis was developed by Pan and coworkers (1983).

An important advantage of the blunt crack band model is that the direction of mesh lines need not be changed if the fracture runs in a skew direction. The crack band propagation criterion then requires some adjustment in order to give results that do not depend on mesh inclination. We consider a rectangular mesh of mesh sizes $\Delta x$ and $\Delta y$ (Figure 13.8). An inclined crack band is represented as a zigzag crack band of overall orientation angle $\alpha_F$. Let $\alpha_M$ be the orientation angle of the mesh lines $x$, and $\alpha_C$ be the direction of the cracks within the finite element (Figure 13.8). We seek the effective width $w_{ef}$ of a smooth crack band that is equivalent to the zigzag band. Consider one cycle, of length $l$, on the line connecting the centroids of the elements in the zigzag band. The number of elements per cycle $l$ in the $x$-direction is $N_x = l\cos\alpha/\Delta x$, and the number of those in the $y$-direction is $N_y = l\sin\alpha/\Delta y$ in which $\alpha = |\alpha_F - \alpha_M|$ provided that $0 \leqslant \alpha \leqslant 90°$. The area of the zigzag band per cycle $l$ is $(N_x\Delta y)\Delta x + (N_y\Delta_x)\Delta y$. This area must equal the area



$lw_{ef}$ of the equivalent smooth crack band, in order to assure the same energy content at the same stresses. This condition yields the effective width

$$w_{ef} = \Delta x \sin\alpha + \Delta y \cos\alpha \quad (0 \leqslant \alpha \leqslant 90°) \tag{13.9}$$

A somewhat different equation, giving similar results for $\alpha \leqslant 45°$, has been used in previous work (Bažant and Cedolin, 1980, 1983a; Cedolin and Bažant, 1980).

A different adjustment is needed when one considers a sudden stress drop and determines crack propagation directly from the energy change $\Delta U$ caused by extending the crack band into the next element. The propagation condition then is $\Delta U/\Delta a = -G_f$ where $\Delta a$ is the length of extension of the crack band, which is equal to the mesh size $h$ if the crack band propagates parallel to the mesh line (Bažant and Cedolin, 1979, 1980; Bažant, 1984). In the case of a zigzag band, $\Delta a$ must be replaced by an effective crack band extension $\Delta a_{ef}$ in the direction of the equivalent smooth crack band. We may assume $\Delta a_{ef}$ to be the same for each crack band advance within the cycle $l$ in Figure 13.8, whether this advance is in the $x$- or $y$-direction. Then $\Delta a_{ef} = l/N$ where $N = N_x + N_y$ = number of elements per cycle $l$. This condition yields

$$\Delta a_{ef} = \left(\frac{\cos\alpha}{\Delta x} + \frac{\sin\alpha}{\Delta y}\right)^{-1} \quad (0 < \alpha < 90°) \tag{13.10}$$

It has been demonstrated that the calculation results are objective not only with regard to the choice of element size but also with regard to the choice of mesh inclination relative to the fracture direction. Meshes of various inclination have been used to calculate the load versus crack-length diagram for the rectangular panel considered before; they have been found to yield essentially the same results, except that the scatter (numerical errors) are somewhat larger for the zigzag crack bands than for a smooth band; see Bažant and Cedolin (1983a).

It is one problem when the fracture direction is known and the zigzag crack band

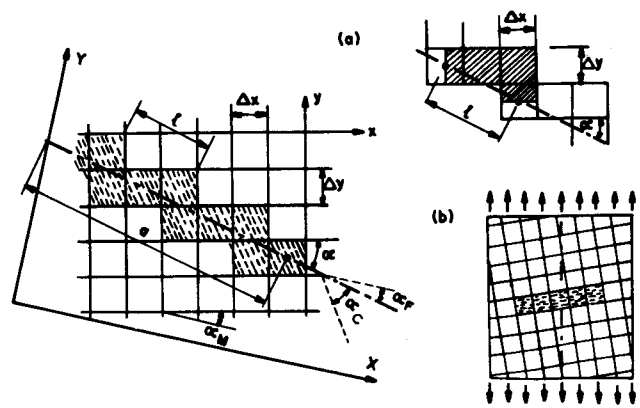


Figure 13.8 Zigzag crack band propagation through a square mesh

is placed so as to conform to the average fracture direction, and another problem when the fracture direction is unknown in advance and a choice of the next element to crack must be made. The latter problem is obviously more difficult. It has been found that any finite element mesh, including a square mesh, is not entirely free of a directional bias. This bias is the strongest when the angle of fracture direction with the mesh line is small. For example, if a square mesh in the centre-cracked rectangular panel is only moderately slanted (Figure 13.8(b)), then the equivalent strength criterion with the effective width given by Equation (13.8) indicates the crack band to extend straight along the mesh line, i.e. in the inclined direction, while correctly there should be side jumps so that the zigzag band would, on the average, conform to a horizontal direction. It appears rather difficult to avoid this type of bias. Various methods to avoid it are being studied (Marchertas *et al.*, 1982; Pan and Marchertas, private communication; Bažant and Pfeiffer, in preparation; Bažant *et al.*, 1983b), and various search routines to determine which element is the next to crack (i.e. the element straight ahead or the element on the left or on the right) are being investigated.

When concrete is reinforced, attention must also be paid to the question of bond slip of reinforcing bars embedded in concrete. It has been shown (Bažant and Cedolin, 1980), that neglect of the bond slip is impossible, leading to unobjective results strongly dependent on the mesh size and converging to a physically incorrect solution. If no slip is considered to occur at the nodes between the bars and concrete, and if the element size is varied, then the stiffness of the connection between the opposite sides across the crack band changes with the mesh size and would approach infinity for a vainishing mesh size, thus preventing any crack propagation at all. In reality, due to a limit on the bond stress that can be transmitted at the surface of steel bars, there is a certain bond slip length $L_s$ on each side of a crack band (Figure 13.9). This length depends on

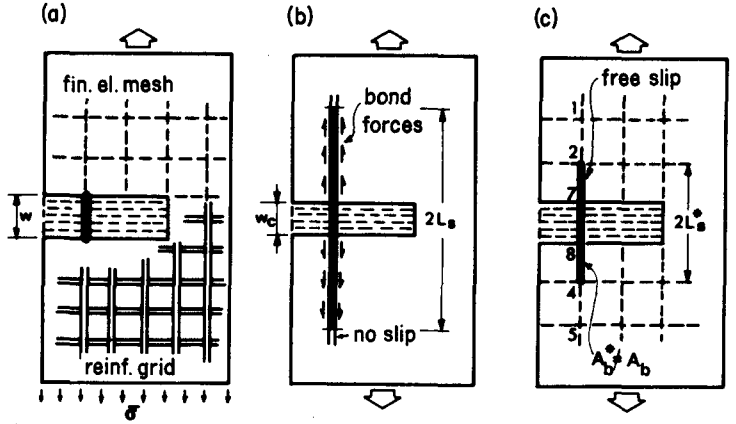


Figure 13.9 Illustrations of bond slip and equivalent free bond slip length (after Bažant and Cedolin, 1980)



the bar cross-section $A_b$, ultimate bond force $U_b'$, ratio $n'$ of the elastic moduli of steel and concrete, stress $\sigma_s$ in the bars at the point of crack band crossing, and the reinforcement ratio $p$ (the bars are assumed to be spaced regularly and densely). The following approximate expression was derived (Bažant and Cedolin, 1980),

$$L_s = \frac{A_s}{U_b'}(\sigma_s - \sigma_s') \simeq \frac{A_b}{U_b'}\frac{1-p}{1-p+n'p}\sigma_s \tag{13.11}$$

For convenience of programming it is further possible to replace this actual bond slip length with an equivalent free bond-slip length $L_s^*$ which coincides with a distance between certain two nodes of the mesh, and which permits neglecting the bond shear stresses, which are difficult to model in a finite element code. The cross-section area $A_b$ must also be adjusted to a value $A_b^*$. The values of $L_s^*$ and $A_b^*$ are then determined from the condition that the extension of the steel bar over the length $L_s$, with bond shear stresses present, would be the same as the extension of a bar of cross-section area $A_b^*$ and length $L_s^*$ with zero bond stresses; (see Bažant and Cedolin, 1980).

When reinforcement is used, the expression for the equivalent strength must also be modified. The following formula has been derived from energy release considerations (Bažant, 1984; Bažant and Cedolin, 1983a).

$$f_{eq}' = c_f\left(\frac{2G_f E_c}{w_{ef} r_f}\right)^{1/2}\left(1 + c_p n' \frac{p}{L_s^*}\cos\alpha_s\right) \tag{13.12}$$

in which $\alpha_s$ = angle of the reinforcing bars with the normal to the crack band, and $c_p$ is an empirical coefficient to be found by numerical calibration, i.e. by comparisons of results for different mesh sizes (Bažant and Cedolin, 1983a).

It might be more realistic to treat reinforcement and bond slip by introducing two overlaid continua, one representing the plain concrete, and one representing the reinforcement mesh. These continua would be allowed to displace relative to each other and would transmit distributed volume forces from one to another, depending on the relative slip. This approach would be, however, much more complicated.

## 13.4 STRUCTURAL SIZE EFFECT

The dispersed and progressive nature of cracking at the fracture front may be taken into account by introducing the following hypothesis (Bažant, 1983a): The *total potential energy release* $W$ *caused by fracture in a given structure depends on both:*

(1) the length $a$ of the fracture, and
(2) the area of the cracked zone, $nd_a a$

in which $n$ is a material constant characterizing the width of the cracking zone at

the fracture front (Bažant and Oh, 1983a), $n \simeq 3$. The dependence of $W$ upon crack length a describes that part of energy release that flows into the fracture front from the surrounding uncracked regions of the structure.

Parameters $a$ and $nd_a a$ are not nondimensional. They are permitted to appear only in a nondimensional form, which is given by the following nondimensional parameters

$$\alpha_1 = \frac{a}{d}, \quad \alpha_2 = \frac{nd_a a}{d^2} \tag{13.13}$$

They represent the nondimensional fracture length and the nondimensional area of the cracked zone. Furthermore, $W$ must be proportional to volume $d^2 b$ of the structure, $b$ denoting the thickness, and to the characteristic energy density $\sigma_N^2/2E_c$ in which $\sigma_N = P/bd$ = nominal stress at failure, $P$ = given applied load, and $d$ = characteristic dimension of the structure. Consequently we must have

$$W = \frac{1}{2E_c}\left(\frac{P}{bd}\right)^2 bd^2 f(\alpha_1, \alpha_2, \xi_i) \tag{13.14}$$

in which $f$ is a certain continuous and continuously differentiable positive function, and $\xi_i$ represent ratios of the structure dimensions characterizing the shape of the structure.

To illustrate the structural size effect, we now consider structures of different sizes but geometrically similar shape, including the same ratio of fracture length to the characteristic dimension of the structure, and the same reinforcement ratio. Under this assumption, the shape parameters $\xi_i$ are constant. Using the energy criterion for crack band propagation, $\partial W/\partial a = G_f b$, in which $G_f$ is the fracture energy, we obtain (for constant $\xi_i$) $\partial f/\partial a = f_1(\partial\alpha_1/\partial a) + f_2(\partial\alpha_2/\partial a)$ where we introduce the notations $f_1 = \partial f/\partial\alpha_1, f_2 = \partial f/\partial\alpha_2$. Substituting this and Equation (13.14) into $\partial W/\partial a = G_f b$, we then get

$$\left(\frac{f_1}{d} + \frac{f_2 nd_a}{d^2}\right)\frac{P^2}{2bE_c} = G_f b \tag{13.15}$$

Here the fracture energy may be expressed as the area under the tensile stress–strain curve, i.e. $G_f = nd_a(1 - E_c/E_t)f_t'^2/2E_c$, in which $E_c$ is the initial Young's elastic modulus of concrete, $E_t$ is the mean strain-softening modulus, which is negative, and $f_t'$ is the direct tensile strength of concrete. Substituting this expression for $G_f$ together with the relation $P = \sigma_N bd$ into Equation (13.15), we finally obtain the following simple formula

$$\sigma_N = Bf_t'\left(1 + \frac{d}{\lambda_0 d_a}\right)^{-1/2} \tag{13.16}$$

in which $\sigma_N$ = nominal stress at failure, $B = [(1 - E_c/E_t)/f_2]^{1/2}$, and $\lambda_0 = mf_2/f_1$.



$B$ and $\lambda_0$ are constants when geometrically similar structures of different sizes are considered.

In the plot of log $\sigma_N$ versus $\log(d/d_a)$ where $d/d_a$ is the relative structure size, Equation (13.16) is represented by the curve shown in Figure 13.10. If the structure is very small, then the second term in the parenthesis in Equation (13.15) is negligible compared to 1, and so $\sigma_N = Bf_t'$ is the condition characterizing failure; it represents the strength criterion, which in Figure 13.10 corresponds to a horizontal line. This special case is obtained if $W$ depends only on the crack-zone area but not on the fracture length.

If the structure is very large, then 1 is negligible compared to the second term in the parenthesis of Equation (13.10). Then $\sigma_N = \text{const.}/\sqrt{d}$. This is the type of size effect known to apply for linear elastic fracture mechanics. Thus, linear elastic fracture mechanics must always apply for a sufficiently large concrete structure, which is no doubt the case for a dam. It is interesting to note also that the preceding nondimensional analysis yields this limiting case when the starting

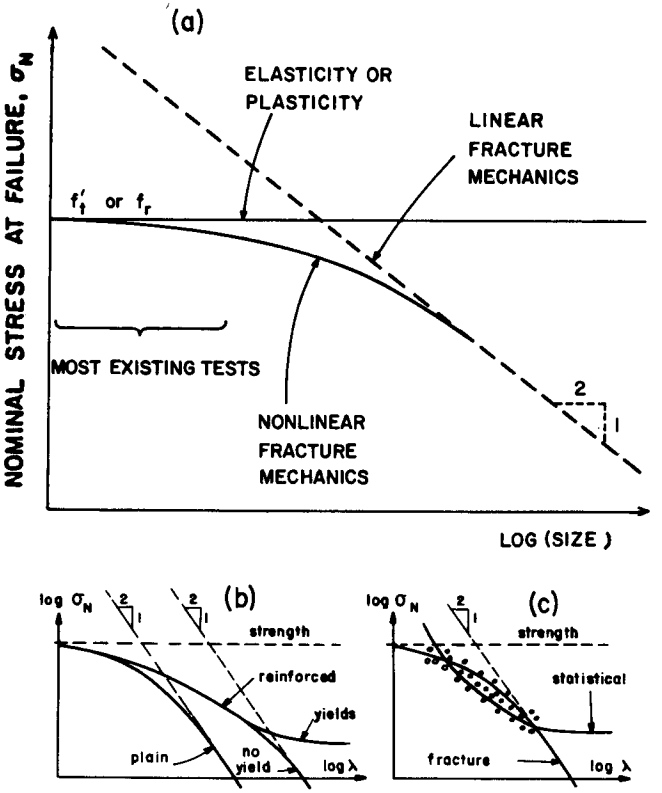


Figure 13.10 Various theories for structural size effect

hypothesis includes only the dependence of $W$ on the fracture length but not on the cracked zone area. In Figure 13.10 the limiting case of linear fracture mechanics is represented by the straight line of downward slope $-1/2$.

The size effect in concrete structures failing due to cracking of concrete represents, as we have shown, a gradual transition from the strength criterion to the energy criterion of linear elastic fracture mechanics. Unfortunately, among the numerous test data on fracture of plain concrete as well as on brittle failures of concrete structures, as reported in the literature, only a very small fraction of the data involves specimens of sufficiently different sizes to check our preceding conclusion on the size effect. Among the available data on plain concrete, the size effect may be checked from the test data of Walsh (1972) (Figure 13.5). A very good agreement with Equation (13.16) is found from these data. As for brittle failure of concrete structures, a check can be made using certain data for the diagonal shear failures of concrete beams with longitudinal reinforcement but without stirrups. Results of such tests are shown in Figure 13.11 for the test data from Kani (1966), Leonhardt and Walther (1961–63), Bhal (1968), Walraven (1978), Taylor (1972), Rüsch *et al.* (1962), and Swamy and Qureshi (1971). In spite of the large scatter, which is due to comparing test data from different laboratories for different concretes, the declining trend is obvious. A horizontal line, corresponding to the strength criterion (as well as to the present ACI or CEB-FIP codes), is contradicted by the test data. At the same time, however, one can clearly see a substantial deviation from the straight line representing linear elastic fracture mechanics. For more detail, see Bažant and Kim (1984).

In the preceding analysis we have not paid any particular attention to reinforcement. If a densely and regularly distributed reinforcement is present, one finds that the size effect is again governed by Equation (13.16), however, with different constants, provided that the reinforcement remains elastic. Compared to plain concrete, the asymptotic straight line for linear elastic fracture mechanics is pushed in the plot of Figure 13.10 toward the right, i.e. there exists a greater range of sizes for which the strength criterion applies. Nevertheless, for sufficiently large structures, a transition to the size effect of linear fracture mechanics does occur. This conclusion, however, is true only as long as the reinforcement does not yield. If it does, then there is another transition in Figure 13.10 to a horizontal asymptote (see Bažant, 1983a).

The decrease of nominal stress at failure with the structure size has been explained in the past as a statistical phenomenon. The strength of concrete is randomly variable, and in a larger structure there is a greater chance of encountering a smaller strength, which could explain the size effect. However, since the random variations occur only within certain representative volumes of a fixed small size, the statistical size effect must lead to a horizontal asymptote. Thus, the asymptotic behaviour is quite different from that we obtained for fracture mechanics. Needless to say, the fracture-type size effect appears to be more realistic.



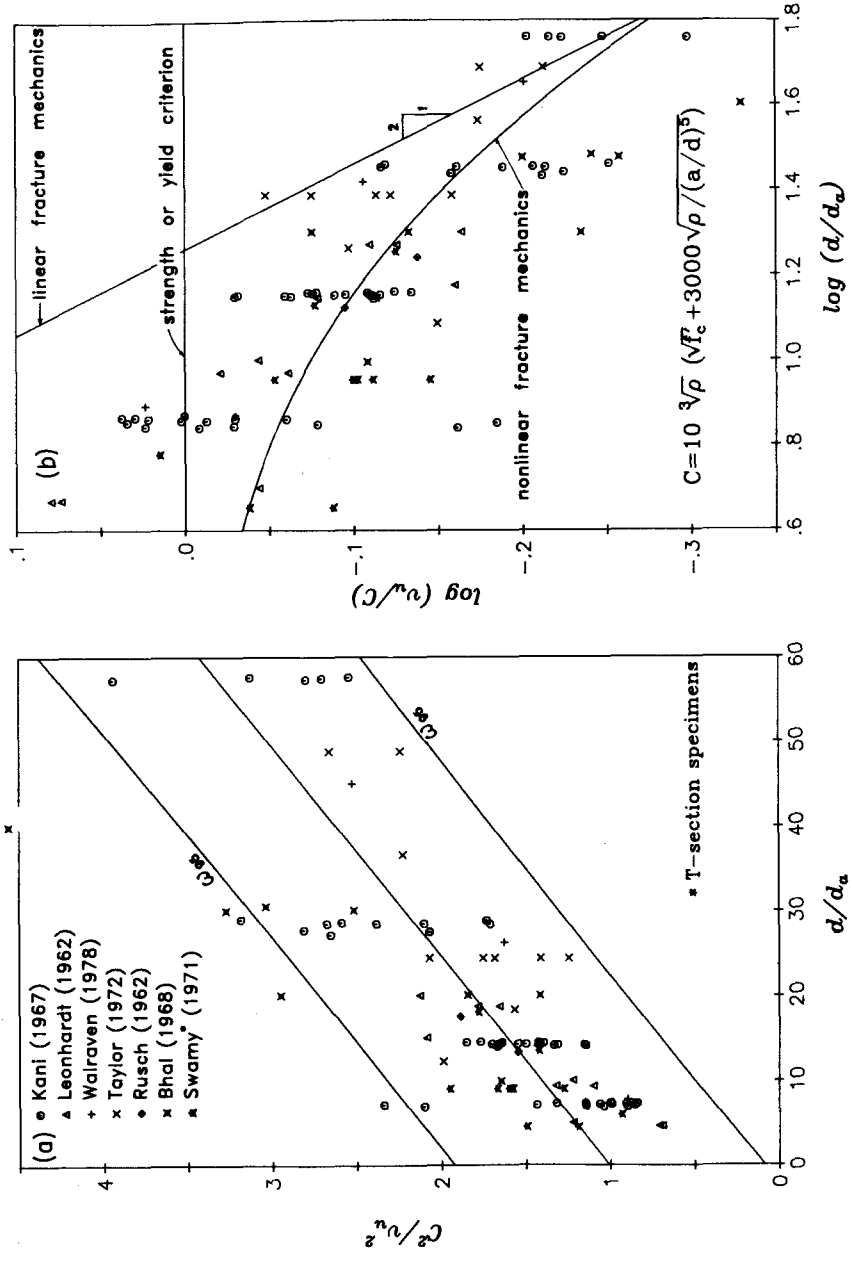


Figure 13.11 Test data from various laboratories on diagonal shear failure of beams reinforced longitudinally but without stirrups (after Bažant and Kim, 1984)

## 13.5 IMBRICATE CONTINUUM AND CONVERGENCE AT MESH REFINEMENT

A limiting and awkward feature of the crack-band theory is the fact that the finite element is not allowed to be smaller than a certain characteristic size $w_c$ (unless, of course, the strain-softening slope is altered, but this is an artifice). This makes it impossible to obtain resolution of the displacement, strain, and stress fields on smaller scales, and particularly near the fracture front. Even though the actual stresses and strains are randomly scattered on such a small scale, their mean description is of interest for the overall response. Moreover, it is of interest from the mathematical point of view. A discrete model is not a mathematically rigorous concept if the discretization cannot be refined and a convergence to some continuum solution achieved. We will now describe a new type of a continuum which extends the crack-band theory to arbitrarily small meshes and achieves a convergent behaviour.

For statistically heterogeneous materials, the overall, averaged behaviour is defined for the so-called representative volume, which represents the smallest sample of the material for which the statistical properties of the microstructure are roughly the same regardless of the location from which the sample is taken. The microscopic, smoothed-out stress $\sigma$ represents the force resultant over the cross-section of the representative volume divided by the cross-section area, and the microscopic, smoothed-out strain, which may be called the mean strain, may be defined as the relative change of length of line segment $\overline{12}$ in Figure 13.12 and may be expressed as

$$\bar{\varepsilon}(x)=\frac{1}{l}\left[u\left(x+\frac{l}{2}\right)-u\left(x-\frac{l}{2}\right)\right] \tag{13.17}$$

Here $x$ = coordinate, $u$ = displacement (macroscopic, smoothed-out), and $l$ = characteristic length = size of the representative volume. Equation (13.17) means that $\bar{\varepsilon}$, as well as associated stress $\sigma$, refers to the cross-section $\overline{PQ}$ in the middle of segment $\overline{12}$ in Figure 13.12. Note that the stress and strain at cross-section $\overline{PQ}$ does not depend on the change of length of line segment $\overline{34}$ (Figure 13.12); rather, the length change of this line segment determines the stress at cross-section $\overline{RS}$. This fact may be expressed by means of the following hypothesis.

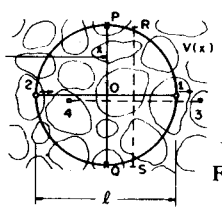


Figure 13.12 Illustrations for representative volume of a heterogeneous aggregate material



*Hypothesis I.* The stress $\sigma(x)$ at any point $x$ (except in a boundary layer of thickness $l$) depends on the change of distance between points $x+l/2$ and $x-l/2$, but does not depend on the change of distance between any other two points lying a finite distance apart.

According to this hypothesis, we may construct the following finite element system for the special case of one-dimension. We consider a bar of unit cross-section (Figure 13.13(a)) and subdivide the length coordinate $x$ by nodes $k=1,2,3,\ldots$ into equal segments of length $h$, subjected to the condition that $h=l/n$ where $n$ is an integer. According to the hypothesis, the stress at point $x_k+l/2$, denoted as $\sigma_k$, depends on the difference of displacements at points $x_k+l$ and $x_k$, i.e.

$$\sigma_k=\bar{E}(\bar{\varepsilon}_k)\varepsilon_k,\quad \bar{\varepsilon}_k=\tfrac{1}{2}(u_{k+n}-u_k) \tag{13.18}$$

in which the subscripts refer to nodal numbers ($k=1,2,\ldots$), and $\bar{E}$ is the secant modulus depending on the mean strain. It is now evident that if $h<l$ (i.e. $n>1$), the mean strain $\bar{\varepsilon}_k$ represents the strain in a finite element which spans from node $k$ to node $k+n$ and *skips* the nodes lying in between, as illustrated in Figure 13.13(b). Since there must be an element of length $l$ attached to every node, the finite elements must obviously overlap, i.e. be imbricated; see the finite elements illustrated by circles in Figure 13.13(b). Due to this imbricate structure, we will call the limiting continuum for $h\to 0$ (or $n\to\infty$) the *imbricate* continuum. A two-dimensional generalization is illustrated in Figure 13.14(a).

It must now be observed, however, that the system of imbricate elements alone (i.e. the circular elements in Figure 13.13(b)) is not stable. One can easily check that the displacement distribution $u_k=A\sin(2\pi x_k/l)$ results in no stress in any imbricate element, i.e. an unresisted deformation can happen, which is in-

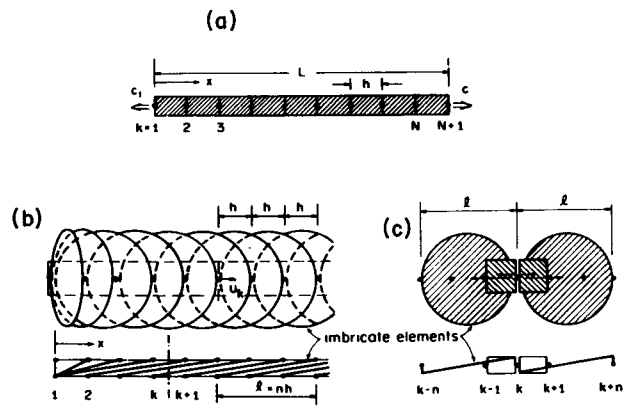


Figure 13.13 (a) Discretization of a one-dimensional bar. (b), (c) Arrangement of imbricate elements

admissible. Therefore, the discrete model must be stabilized by introducing additional finite elements of the smoothed-out macroscopic continuum which have length $h$ and span from one node to the next (Figure 13.13(a)–(c)). These are the usual finite elements, and they will be called the local elements. The sum of the cross-section areas of these local elements and of the imbricate elements must equal 1. Denoting as $c$ the cross-section (or thickness) of the local elements ($0 < c \leqslant 1$), we must assure that the combined cross-section area of the imbricate elements equals $1 - c$. Because $n$ imbricate elements intersect any cross-section between two nodes (Figure 13.13(b)), the cross-section area or thickness of each imbricate element must be taken as

$$b_e = \frac{1-c}{n} \tag{13.19}$$

As the mesh is refined ($n \to \infty$), the thickness of each imbricate element approaches zero.

Even though $n$ imbricate elements intersect each cross-section, there are only two imbricate elements attached to one node $k$ (Figure 13.13(c)). In addition, there are two local elements attached to node $k$. Thus, the nodal equilibrium equation reads $b_e(\sigma_k - \sigma_{k-n}) + c(\tau_k - \tau_{k-1}) + p(x_k)h = 0$, in which $p$ is the distributed load per unit length, and $\tau_k$ is the stress in the local element, which may be expressed as

$$\tau_k = E(\varepsilon_k)\varepsilon_k, \quad \varepsilon_k = \frac{1}{h}(u_{k+1} - u_k) \tag{13.20}$$

Here $E$ is the local elastic modulus, interpreted as a secant modulus which depends on the local strain $\varepsilon_k$.

Substituting, according to D'Alembert principle, $p(x_k) = \rho\ddot{u}_k$ where superior dots denote time derivatives and $\rho$ is the mass density, and rearranging algebraically the foregoing node equilibrium equation, we obtain the following equation of motion

$$\frac{1-c}{l^2}[\bar{E}(\bar{\varepsilon}_k)(u_{k+n} - u_k) - \bar{E}(\bar{\varepsilon}_{k-n})(u_k - u_{k-n})] + \frac{c}{h^2}[E(\varepsilon_k)(u_{k+1} - u_k) - E(\varepsilon_{k-1})(u_k - u_{k-1})] = \rho\ddot{u}_k \tag{13.21}$$

Although elastic materials are not the purpose of this formulation, it is interesting to note that for the special case of constant $\bar{E}$ and $E$, Equation (13.21) reduces to

$$(1-c)\bar{E}\frac{u_{k+n} - 2u_k + u_{k-n}}{l^2} + cE\frac{u_{k+1} - 2u_k + u_{k-1}}{h^2} = \rho\ddot{u}_k \tag{13.22}$$

The total stress, representing the sum of all forces within the cross-section of the bar, may be expressed as

$$S_k = \frac{1-c}{n}\sum_{j=1}^{n}\sigma_{k+1-j} + c\tau_k \tag{13.23}$$



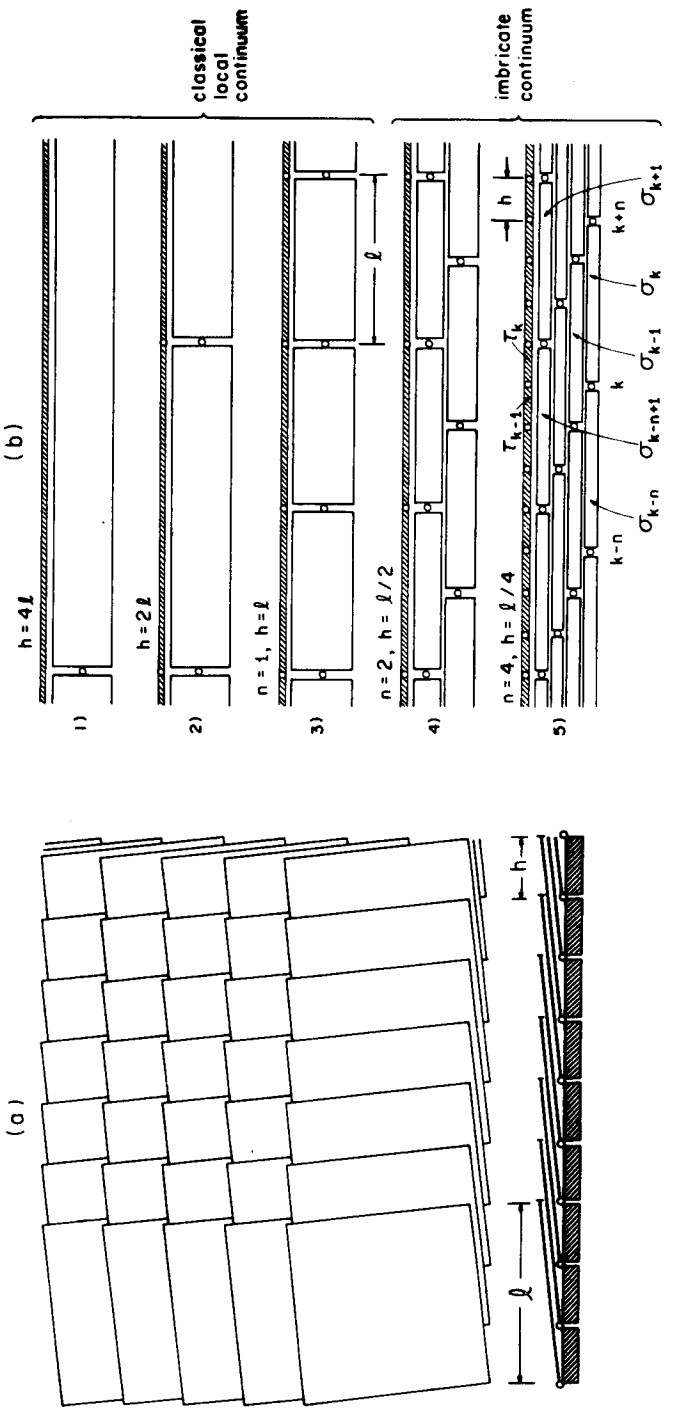


Figure 13.14 (a) Two-dimensional arrangement of square imbricate elements (the element sides should be perfectly horizontal and vertical but are misaligned for the purpose of illustration). (b) One-dimensional element arrangements for finer and finer subdivisions (the nodes on top of each other have the same displacement)

It is now obvious that the finite difference expressions in Equation (13.22) represent the well-known finité difference approximations to the second derivative $\partial^2 u/\partial x^2$. Similarly, finite difference approximations of the first derivatives may be detected in Equation (13.21). Thus, the continuum limit of Equation (13.21) ($h \to 0$ and $n \to \infty$ at constant $l$) has the form

$$(1-c)D_x\sigma(x) + c\frac{\partial}{\partial x}\tau(x) = \rho\frac{\partial^2 u(x)}{\partial t^2} \quad \left(\text{for} \frac{l}{2} \leqslant x \leqslant L - \frac{l}{2}\right) \tag{13.24}$$

in which

$$\sigma(x) = \bar{E}D_x u(x), \quad \tau(x) = E\frac{\partial}{\partial x}u(x) \tag{13.25}$$

with $D_x$ denoting an operator defined by the relation

$$D_x u(x) = \frac{1}{l}\left[u\left(x+\frac{l}{2}\right) - u\left(x-\frac{l}{2}\right)\right] = \bar{\varepsilon}(x) \tag{13.26}$$

Here $t$ = time, $\sigma$ is the limit of the stress in the imbricate elements which may be called the broad-range stress (note that it does not represent a mean of some stresses, unlike $\bar{\varepsilon}$), and $\tau$ is the limit of the stresses in the local elements which may be called the local stress. Equations (13.24)–(13.26) are the continuum relations characterizing the imbricate continuum. The total stress in the continuum is obtained as the limit of Equation (13.23),

$$S(x) = \frac{1-c}{l}\int_{-l/2}^{l/2} \sigma(x+s)\mathrm{d}s + c\tau(x) = (1-c)\,\bar{\sigma}(x) + c\tau(x) \tag{13.27}$$

in which $\bar{\sigma}$ represents the mean broad-range stress. Note that Equation (13.24) may be also written as $\partial S(x)/\partial x = \rho\ddot{u}(x)$.

The question now is whether the imbricate continuum can, indeed, describe strain-softening regions of finite size, and whether it can do so in a stable manner. It appears that, in order to achieve stability, the local stress–strain relation must not exhibit strain-softening, i.e. the tangent modulus based on $E(\varepsilon)$ must be positive, while the broad stress–strain relation may exhibit strain-softening, i.e. the tangent modulus $\bar{E}_t = \bar{E} + (\partial\bar{E}/\partial\bar{\varepsilon})\bar{\varepsilon}$, may become negative. The question of stability is easy to investigate by considering the broad stress–strain relation $\sigma = \bar{E}_t(\bar{\varepsilon} - \varepsilon_f)$ is which $E_t$ and $\varepsilon_f$ are constants. Then, substituting $u = A\exp[\mathrm{i}\omega(x - vt)]$ where $\mathrm{i}^2 = -1$, and $\omega, v, A$ are constants, one finds that the field equation in Equations (13.24)–(13.26) for $E = \bar{E}$ = constant reduces to an algebraic equation for the wave velocity $v$. As is well-known, the continuum is stable if $v$ is not imaginary, i.e. $v^2 > 0$. It can be shown that this leads to the condition $c > 0$.

Computer calculations (Bažant *et al.*, 1983b) verified that $c = 0.1$ yields a stable and well behaved solution. This is true even for strain-softening with tangent



modulus $\bar{E}_t = -0.2E$ where $E$ is the elastic modulus of the material. In these calculations, carried out by T. P. Chang (Bažant *et al.*, 1983b), two broad-range stress–strain diagrams were considered: one which dips below the strain axis so as to achieve full strain-softening for the total stress $S$, and one which terminates by a horizontal segment when it reaches the strain axis, in which case the total stress $S$ does not reach full strain-softening (Figure 13.15). In both cases, for strains exceeding strain $\varepsilon_f$ at the end of strain-softening, a horizontal plateau is considered both for the broad-range and the local stress–strain diagram (Figure 13.15). Of these, the case where the strain-softening does not dip below the strain axis appears physically more reasonable, but both approaches appear to work numerically (Bažant, Chang and Belytschko, 1983b).

The field equations in Equations (13.24)–(13.26) apply only at distances more than $l$ from the boundary. Within boundary segments of length $l$, the continuum equations are much more complicated, however, the discrete modelling is quite simple. One needs to first lay out all imbricate elements attached to every node, and then those imbricate elements which stick out beyond the boundary may be chopped and attached to the boundary node (see Figure 13.13(b)).

For the stress–strain diagrams in Figure 13.15, extensive computer studies of convergence at diminishing mesh size $h$ have been carried out (Bažant *et al.*, 1983b). As a practical example, it was considered that constant outward velocities $c_1$ in the outward direction are prescribed at the boundary nodes; Figure 13.13(a). For the case of an elastic bar, this produces step waves of strain with magnitudes $c_1/v$; as these two waves meet at mid-length, the strain is doubled. For the case of a strain-softening continuum (Figure 13.15), the velocity $c_1$ is selected such that the initial inward step-waves are just below the elastic strain limit. As these two waves meet at mid-length, strain rapidly increases into the strain-softening range. Examples of some results (Bažant *et al.*, 1983b), showing strain distributions for various times obtained for various local element sizes $h$, are exhibited in Figure 13.16(a). These figures demonstrate that a finite-size strain-softening region is obtained, and that the response converges as $h$ is diminished. Moreover, it has

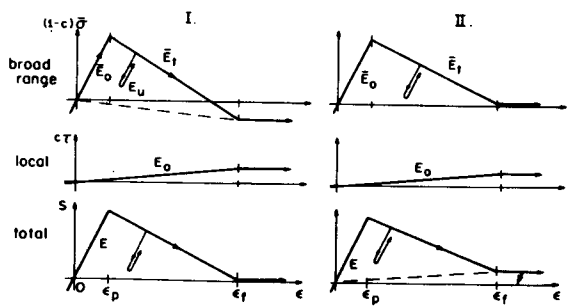


Figure 13.15 Broad-range, local and total stress–strain relations used in numerical example

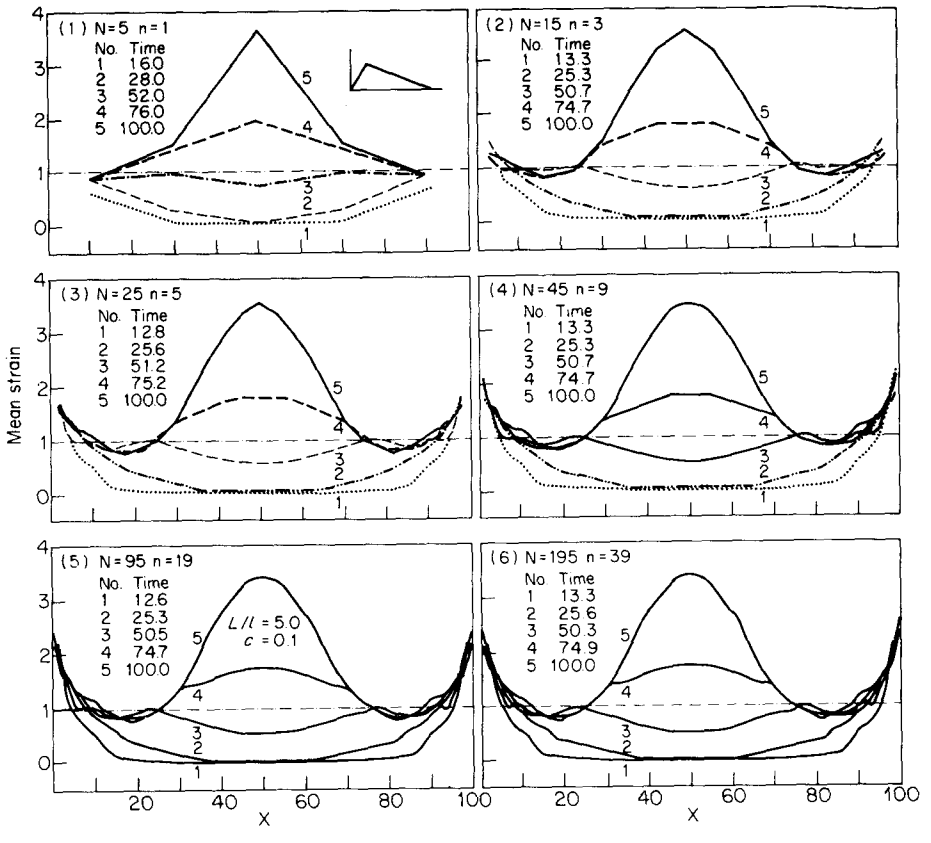


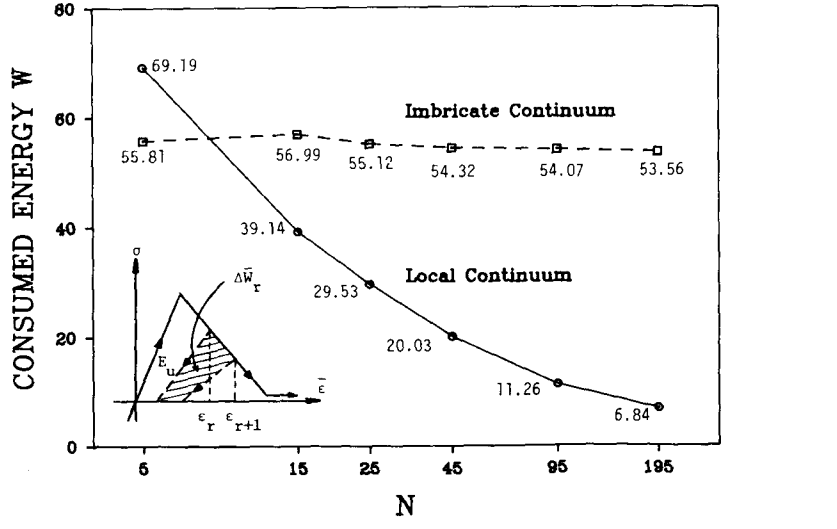


Figure 13.16 Mean strain distributions at various times obtained by T. P. Chang (Bažant *et al.*, 1983b) for various numbers $N$ of imbricate continuum subdivisions and energy dissipated by strain-softening as a function of $N$.



been checked that for the case of the usual, local continuum ($l = h$ at diminishing $h$), the solution converges to an exact solution for strain-softening in this bar, obtained in Bažant and Belytschko (1983). These results have been obtained by an explicit time-step algorithm (Bažant, Chang and Belytschko, 1983b).

Particularly interesting is a comparison of the total energy $W$ dissipated in the bar due to strain-softening. Figure 13.16(b) shows a plot of $W$ as a function of the number $N$ of subdivisions; $W$ is obtained from $\bar{W}_r = [(\sigma_r^2/E_r') - (\sigma_{r+1}^2/E_{r+1}') + (\sigma_r + \sigma_{r+1})\Delta\varepsilon]/2$ = energy dissipated per step and per unit length, $E_r'$ = unloading modulus at time $t_r$. Note that for the imbricate continuum $W$ converges to a finite value while for the classical local continuum it converges to zero, which is unrealistic.

A more rigorous derivation of the imbricate continuum may be based on the principle of virtual work. It follows directly from Hypothesis I that the work variation for a one-dimensional bar of length $l$ may be expressed as

$$\delta W = \int_{l/2}^{L-l/2} \left\{ \frac{\sigma(x)}{l}\left[\delta u\left(x+\frac{l}{2}\right) - \delta u\left(x-\frac{l}{2}\right)\right] + \tau(x)\frac{\partial}{\partial x}\delta u(x) - p(x)\delta u(x) \right\} dx + \delta W_b = 0 \tag{13.28}$$

in which $\delta u$ is any kinematically admissible variation of displacements, and $\delta W_b$ is the virtual work done within the boundary segments of length $l$. It may be shown by variational calculus that the condition $\delta W = 0$ for any $\delta u$ leads to the continuum equations in Equations (13.24)–(13.26) (Bažant, 1983b).

The variational approach permits deriving the field equations for the imbricate continuum in three-dimensions. For this purpose, the operator $D_s$ may be generalized as

$$D_i u_j\left(\mathbf{x}+\frac{l}{2}\mathbf{i}\right) = \frac{1}{l}\left[u_j\left(\mathbf{x}+\frac{l}{2}\mathbf{i}\right) - u\left(\mathbf{x}-\frac{l}{2}\mathbf{i}\right)\right]a_i \tag{13.29}$$

in which subscripts $i,j$ refer to cartesian coordinates $x_i (i = 1, 2, 3)$, $u_j$ are the displacement components, $\mathbf{i}$ is the unit vector of axis $x_i$, $a_i$ are the direction cosines of vector $\mathbf{i} = (1, 0, 0)$ or $(0, 1, 0)$ or $(0, 0, 1)$, and $\mathbf{x}$ is the coordinate vector. The mean strain may then be generalized as

$$\bar{\varepsilon}_{ij} = \tfrac{1}{2}(D_i u_j + D_j u_i) \tag{13.30}$$

From Hypothesis I it follows that stresses $\sigma_{ij}$ in a three-dimensional generalization of the imbricate continuum must depend on the mean strains $\bar{\varepsilon}_{ij}$ defined above because these strains depend only on the change of distance between points that lie a distance $l$ apart. Consequently, the principle of virtual work for the imbricate continuum must have the form

$$\delta W = \int_{\Omega'} [(1-c)\sigma_{ij}\delta(D_i u_j) + c\tau_{ij}\delta u_{i,j} - p_i\delta u_i]\,dV + \delta W_b = 0 \tag{13.31}$$

in which repeated subscripts imply summation over 1, 2, 3; a subscript preceded by a comma denotes a partial derivative; $\tau_{ij}$ are local stresses depending on displacement gradients; $p_i$ are applied loads per unit volume; $\Omega'$ denotes the domain of the body excluding a boundary layer of thickness $l/2$; and $\partial W_b$ is the virtual work done by the stresses within this boundary layer. Introducing a certain kind of shift operators, one can isolate the variation $\delta u_j$ from the integrand in the foregoing integral and show that the continuum equations of motion (for $p_i = -\rho\ddot{u}_i$) must have the form (Bažant, 1983b)

$$(1-c)D_j\sigma_{ij} + c\tau_{ij,j} = \rho\ddot{u}_i \qquad (\text{for } \mathbf{x}\in\Omega'') \tag{13.32}$$

in which

$$\sigma_{ij} = \bar{C}_{ijkm}(\bar{\boldsymbol{\varepsilon}})\bar{\varepsilon}_{km} = C_{ijkm}(\bar{\boldsymbol{\varepsilon}})D_m u_k \tag{13.33}$$

Here $\bar{C}_{ijkm}$ are the secant moduli which generally depend on the mean strain tensor $\bar{\boldsymbol{\varepsilon}}$. Equation (13.32) holds only for points within domain $\Omega''$ which represents the domain of the body without a boundary layer of thickness $l$. Within the boundary layer the continuum equations of motion are much more complicated and it is preferable to set up their discretized, finite element form directly. Similarly to $\sigma$, $\sigma_{ij}$ may be called the components of the broad-range stress tensor.

Alternatively, and perhaps more rigorously, the mean strain $\bar{\varepsilon}_{ij}$ can be defined as the average of the strain gradient $u_{i,j}$ obtained by integration over a sphere of diameter $l$ surrounding the given point. It may also be expressed as an integral of $u_i n_j$ over the surface of this sphere (where $n_j$ are the direction cosines of an outward normal of this surface). It may also be defined by least-square fitting of a homogeneous local strain field over the surface of this sphere. All these three definitions are exactly equivalent, but they are only approximately equivalent to the definition of mean strain based on the difference operator in Equation (13.29). However, the use of Equation (13.29) is much simpler for numerical calculations, as well as for deriving the continuum equations of motion from the principle of virtual work (Bažant, 1983b).

Can the difference operators be eliminated? They can, as an approximation, if $u(x)$ is expanded in Taylor series. Then

$$\bar{\varepsilon} = D_x u \simeq u' + \frac{l^2}{24}u''' \tag{13.33a}$$

and the one-dimensional equation of motion within regions in which the tangent moduli $\bar{E}_t$ and $E_t$ are constant becomes

$$\tilde{E}_t\frac{\partial^2 u}{\partial x^2} + (1-c)\bar{E}_t\lambda^2\left(2\frac{\partial^4 u}{\partial x^4} + \lambda^2\frac{\partial^6 u}{\partial x^6}\right) = \rho\frac{\partial^2 u}{\partial t^2} \tag{13.33b}$$

where

$$\tilde{E}_t = (1-c)\bar{E}_t + cE_t, \quad \lambda^2 = l^2/24 \tag{13.33c}$$



The foregoing equations permit obtaining solutions to one-dimensional problems analytically.

To generalize Equation (13.33a) to three dimensions, one may use the Taylor series expansion to obtain

$$D_j u_i(\mathbf{x}) \simeq u_{i,j}(\mathbf{x}) + u_{i,jkm}(\mathbf{x})\frac{1}{2V}\int_{V(\mathbf{x})}(x'_k - x_k)(x'_m - x_m)\,dV' \tag{13.33d}$$

where $V$ is a sphere constituting the representative volume, centered at $(\mathbf{x})$. The integral in the last equation may be expressed as $\delta_{km}l'^2/40$ where $\delta_{km}$ = Kronecker delta and $l'$ = diameter of the sphere. Now we see that if we would set $l' = l$, Equation (13.33d) would not reduce to Equation (13.33a) for the case of uniaxial strain. It is preferable, therefore, to keep the coefficient 1/24, and this may be obtained by setting $l'^2/40 = l^2/24$ as obtained in Equation (13.33a), which yields $l' = l\sqrt{5/3} = 1.29l$. Thus, the tensors of the mean displacement gradient and the mean strain may be approximated as

$$D_j u_i \simeq u_{i,j} + \frac{l^2}{24}u_{i,jkk}, \quad \bar{\varepsilon}_{ij} \simeq \varepsilon_{ij} + \frac{l^2}{24}\varepsilon_{ij,kk} \tag{13.33e}$$

Note also that $\bar{\boldsymbol{\varepsilon}} = \boldsymbol{\varepsilon} + (l^2/24)\nabla^2\boldsymbol{\varepsilon}$, etc., where $\nabla^2$ = Laplacean. The stress difference in the equation of motion (Equation (13.32)) may be approximated as

$$D_j\sigma_{ij} \simeq \sigma_{ij,j} + \frac{l^2}{24}\sigma_{ij,jkk} \tag{13.33f}$$

For the total stress, one can show that

$$S_{ij} = (1-c)(1-\lambda^2\nabla^2)C_{ijkm}(1+\lambda^2\nabla^2)\varepsilon_{km} + c\tau_{ij} \tag{13.33g}$$

and the equation of motion may then be written as $S_{ij,j} = \rho\ddot{u}_i$.

The foregoing approximations by higher-order derivatives might be useful for analytical solutions.

The consequences for the blunt crack band theory can now be discussed. When the mesh size $h$ is chosen equal to the size $l$ of the representative volume, the finite element model of the imbricate continuum becomes equivalent to that of the classical local continuum, as used in the crack band theory. Meshes with $h > l$ (Figure 13.14(b)) make no sense for the imbricate continuum model because their characteristic length cannot be resolved. Therefore, a local continuum theory is the only meaningful basis for the finite element analysis if $h \geqslant l$. On the other hand, finite element analysis based on the local continuum theory makes no sense when $h < l$, and the imbricate continuum is needed for such a refinement of mesh (see Figure 13.14b)).

Due to the fact that for $h = l$ the finite element models for the local and the

imbricate continuum coincide, the characteristic length, $l$, must be the same as the width of the crack band front, $w_c'$, introduced before. This provides a method of experimental determination of $l$.

With the formulation of the imbricate continuum, the continuum theory appears to be put on a rigorous, continuum mechanics basis. Aside from that, the imbricate continuum may be used to calculate the detailed distribution of the smoothed macroscopic stress and strain near the fracture front, or in the vicinity of singularities in general (at concentrated loads, at corners or notches, etc.).

Before leaving this topic, we should at least briefly comment on various recent attempts to model strain-softening by means of either the classical, local continuum or the classical non-local continuum. Strain-softening has been a suspect feature in continuum mechanics ever since Hadamard pointed out that the wave propagation speeds become imaginary when the matrix of the tangent moduli ceases to be positive definite, which is the case for strain softening (Hadamard, 1903; Thomas, 1961). Hadamard's point, however, neglected the fact that different tangent moduli apply to positive and negative increments of strain. This fact was recently taken into account and it was found that the use of strain-softening with a classical, local continuum does not result in a mathematically meaningless formulation.

For example, exact stability analysis has been carried out for one-dimensional strain localization due to strain-softening (Bažant, 1976; Bažant and Panula, 1978) (as opposed to strain-localization instabilities caused by geometrical nonlinearity (Rice, 1976; Rudnicki and Rice, 1975)). It was found that the equilibrium path of the structure is unique and can be traced just as well as the equilibrium path in the buckling of the perfect column. Recently, an exact solution has been obtained for some one-dimensional wave propagation problems with strain softening (Bažant and Belytschko, 1983). Again, it was shown that the solution is unique except for some values of prescribed boundary velocities for which the solution changes discontinuously. In both the static and the dynamic problem, the strain-softening in a classical, local continuum is found to localize immediately into a layer of zero thickness in which the strains become unbounded. Furthermore, the energy consumed by strain-softening failure is found to be zero (Figure 13.16). So the problem with the use of strain-softening in the classical, local continuum theory is not that the formulation would be unsound mathematically, but that the solution is not representative of the behaviour of real strain-softening materials, in which the strain-softening regions have a finite size, and a finite energy is consumed by failures due to strain-softening.

Quite illuminating was the work of Burt and Dougill (1977). They simulated by a computer a random two-dimensional network whose joints were placed at random locations over a rectangular domain. They considered all pairs of joints with a distance less than a certain constant $l$, made a random selection among all such pairs, and introduced connecting pin-jointed elastic struts between each



pair. The stiffnesses and strength limits of these struts were generated randomly according to prescribed normal distributions. After reaching the strength limit, the strut was assumed to fail and its internal force to drop suddenly to zero. Although, due to its neglect of shear resisting elements, this model could not have exhibited a correct elastic Poisson ratio (it was 1/3), the simulated inelastic behaviour was strikingly similar to that of concrete. Especially, strain-softening regions of finite size were obtained in these random networks. This clearly established the need to consider some sort of a non-local continuum.

In the simplest possible non-local continuum theory, and the only one which appears to have been used thus far, the stress at point x is assumed to be a function of the weighted average of strains obtained by integration over a neighbourhood of x. Other relations, particularly the continuum equations of motion in terms of stresses and the strain-displacement relations, are the same as for the classical, local continuum. It appeared, however, that this classical form of the non-local continuum theory (Kröner, 1967, 1968; Krumhansl, 1968; Kunin, 1968; Levin, 1971; Eringen and Edelen, 1972; Eringen and Ari, 1983) is unworkable for the modelling of strain-softening. Computer simulations always resulted in unstable behaviour, and did not exhibit convergence at mesh refinements (T. P. Chang), and strain-softening always localized between two adjacent points of the mesh. It was after this experience that the concept of the present imbricate continuum was conceived.

## 13.6 EQUIVALENT LINEAR ANALYSIS OF FRACTURE

Since uncracked concrete in tension behaves essentially elastically, the stress field surrounding the fracture process zone in concrete should be predominantly elastic. However, it corresponds to some equivalent crack length rather than the actual crack length. Thus, the idea of an equivalent crack length which has no relation to the actual crack length should allow an approximate linear analysis of concrete fracture. As it turns out, however, this is not sufficient. It is also necessary to assume that the fracture energy $G_c$ is variable rather than constant. Now it appears that for many practical purposes the dependence of the fracture energy on structural geometry, type of loading, notch length, etc., can be neglected and only the dependence of the fracture energy on the length $c$ of crack extension from the notch needs to be considered. Thus, the plot of $G_c$ versus $c$ is assumed to be unique and is called the resistance curve or R-curve. This idea, proposed by Irwin (1960) and Krafft *et al.* (1961), has proved to be rather useful for metals (Broek, 1974; Parker, 1981) and appears to work also quite well for concrete (Bažant and Cedolin, 1983b).

Let us briefly review the R-curve concept. We consider that the fracture energy, $G_c$, is a certain given function of the crack extension $c$ from the notch or smooth surface, i.e. $G_c = G_c(c)$ in which $c = a - a_0$, $a_0$ = length of the notch, and $a$ = total length of crack plus notch (Figure 13.17). The energy that must be supplied to the

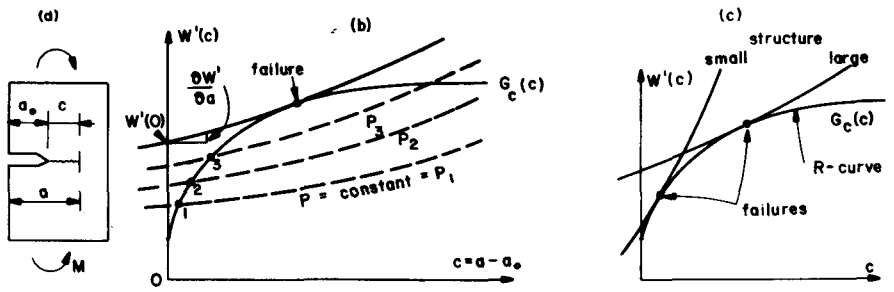


Figure 13.17 Determination failure with the help of R-curve

structure to produce the crack is $U = b\int G_c(c)\,da - W(a)$ where $b$ is the thickness of the structure and $W$ is the total release of strain energy from the structure or specimen. An equilibrium state of fracture occurs when no energy needs to be supplied to change $a$ by $\delta a$ and none is released, i.e. when $\delta W = 0$. Since $\delta U = (\partial U/\partial a)\delta a = 0$ in which $\partial U/\partial a = bG_c - W' = 0$ and $W' = \partial W/\partial a$, it follows that fracture equilibrium occurs when

$$W'(a) = bG_c(c) \qquad \text{(equilibrium)} \qquad (a = a_0 + c) \tag{13.34}$$

The equilibrium fracture state is stable if the second variation $\delta^2 U$ is positive. Since $\delta^2 U = (\partial^2 U/\partial a^2)\delta a^2$ where $\partial^2 U/\partial a^2 = b\partial G_c/\partial a - W''(a)$, and $W''(a) = \partial^2 W/\partial a^2$, the conditions for stability of fracture and the limit of stability, i.e. the failure condition, are given by

$$bG_c'(c) - W''(a) > 0 \qquad \text{(stable)} \tag{13.35a}$$

$$= 0 \qquad \text{(critical)} \tag{13.35b}$$

Considering structures that are geometrically similar but have dissimilar notches, and using dimensional analysis, we may write, in analogy to Equation (13.14),

$$W'(a) = \frac{P^2 g(\alpha)}{E_c b d}, \qquad W''(a) = \frac{P^2 g'(\alpha)}{E_c b d^2} \qquad \left(\alpha = \frac{a}{d}\right) \tag{13.36a, b}$$

in which $d$ is the characteristic dimension of the structure, $E_c$ is the Young's modulus, $P$ is the applied load, and $g(\alpha)$ is a nondimensional function, common to all structures of a similar shape, which can be found for many typical specimens in handbooks and can be always determined by linear finite element analysis. Also, $g'(a) = dg/d\alpha$. Substituting Equations (13.36(a,b)) into Equations (13.34)–(13.35) and eliminating $P$, we find the condition

$$G_c(c)g'(\alpha) - G_c'(c)g(\alpha)\,d > 0 \qquad \text{(stable)} \tag{13.37a}$$

$$= 0 \qquad \text{(critical)} \tag{13.37b}$$



Furthermore, noting that $dg/dc = dg/da = g'(\alpha)/d$, we find that the last form of the critical state condition is equivalent to the following maximizing condition

$$\frac{G_c(c)}{g(\alpha)} = \text{Max} \qquad \left(\alpha = \frac{g_0 + c}{d}\right) \tag{13.38}$$

Thus, the value of crack extension $c$ at failure may be simply found by a search for the maximum of the foregoing expression if functions $G_c$ and $g$ are known. Alternatively, the value of $c$ at failure may be found by solving Equation (13.37b), which would normally be carried out by iterative Newton method.

Analysis of the bulk of fracture test data for concrete available in the literature (Bažant and Cedolin, 1983b) has indicated that failure loads are not very sensitive to the precise shape of the R-curve, i.e. curve $G_c(c)$. Various algebraic expressions have been used for the R-curve $G_c(c)$, including an exponential curve with a horizontal asymptote, a parabola transiting at its apex into a horizontal line, and a bilinear expression. All these expressions have been found to allow roughly equally good fits of the available scattered data. Only the initial value of $G_c$, the final value $G_f$, and the overall slope of the rising portion of the R-curve, have been found to be of importance (Bažant and Cedolin 1983b). This means that at the present level of measurement capabilities it makes no sense trying to determine the R-curve with great precision or to develop sophisticated theories for theoretical determination of the R-curve. From the convenience viewpoint, the following elliptic and parabolic curves are preferable because they facilitate the solution of failure loads;

$$G_c(c) = G_f\left[1 - \beta\left(1 - \frac{c}{c_m}\right)^2\right]^{1/2} \tag{13.39a}$$

$$\text{(for } 0 \leqslant c \leqslant c_m,\ G_c(c) = G_f \text{ for } c \geqslant c_m)$$

$$G_c(c) = G_f\left[1 - \beta\left(1 - \frac{c}{c_m}\right)^2\right] \tag{13.39b}$$

Here $G_g, c_m$ and $\beta$ are constant material parameters. Both these functions permit finding explicit expressions for $c$ and $P$ at failure if the function $g(\alpha)$ is approximated linearly, $g(\alpha) = g_0 + (\alpha - \alpha_0)g_0'$ with $\alpha_0 = (a_0 + c_0)/d$. This linear approximation is always sufficient for large enough structures. Substituting the last expression and Equation (13.39a) or (13.39b) into Equation (13.37b), one can find the following equations for the crack extension $c$ at failure;

$$c = \frac{g(\alpha)d - g'(\alpha)c_0}{g'(\alpha)(c_m - c_0) + g(\alpha)d}c_m \qquad \text{(ellipse)} \tag{13.40}$$

$$(c_m - c)^2 - \left(\frac{2g(\alpha)d}{g'(\alpha)} + c_m - c_0\right)(c_m - c) + \frac{c_m^2}{\beta} = 0 \qquad \text{(parabola)} \tag{13.41}$$

Here $c_0$ and $\alpha_0$ characterize the point about which the R-curve is linearized, and if

$\alpha - \alpha_0$ is small, the approximation of $g(\alpha)$ is very good. After determining $c$ from one of these equations, the value of $P$ at failure may be found from Equations (13.36a) and (13.34).

Let us now check what kind of size effect is implied by the R-curve approach. For the parabolic R-curve, substitution of $P = \sigma_N bd$ and of the linear approximation for $g(\alpha)$, and elimination of $c$ from Equations (13.36a), (13.36b), (13.34), and (13.35b), yields the equation

$$C_1\sigma_N^4 - (C_2 + C_3 d)\sigma_N^2 + G_f = 0 \qquad (P = bd\sigma_N) \tag{13.42}$$

in which

$$C_1 = \frac{b^2 c_m^2 g'^2(\alpha)}{4\beta G_f E_c^2}, \quad C_2 = \frac{b}{E_c}(c_m - c_0)g'(\alpha), \quad C_3 = \frac{b}{E_c}g(\alpha) \tag{13.43}$$

Solving Equation (13.42) for various values of $d$, one can construct the plot of the nominal stress at failure, $\sigma_N$, versus the characteristic dimension $d$; see Figure 13.18 (solid curve). We see that the resulting plot is very close to that obtained previously from dimensional analysis (Equation 13.16); see Figure 13.18 (dashed curve). This agreement lends support to the use of the simple parabolic formula for the R-curve. The function $g(\alpha)$ used in Figure 13.18 is that which corresponds to a three-point bent specimen used by Walsh (1972), for which the beam span-to-depth ratio is 4, and the notch depth to beam depth ratio is 1/3. This function is

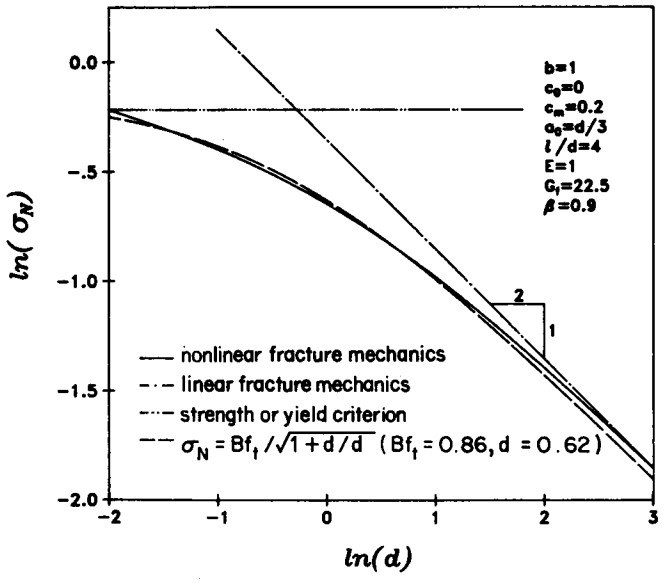


Figure 13.18 Structural size effect obtained from parabolic R-curve, and its comparison with Equation (13.16)



(Tada *et al.*, 1973) $g(\alpha) = \pi(L/d)^2\alpha(1.634 - 2.603\alpha + 12.30\alpha^2 - 21.27\alpha^3 + 21.86\alpha^4)^2$, where $L$ = beam span and $d$ = beam depth.

To illustrate the degree of agreement with test data which can be achieved with the parabolic R-curve, Figure 13.19 reproduces from Bažant and Cedolin (1983b) a plot of the theoretical versus measured values of $P$ at failure, normalized with regard to the failure load $P_0$ calculated from the strength theory. If the theory were perfect, the data points would have to fall on a straight line through the origin, having slope 1. The deviations from such a straight line represent errors. Statistical regression analysis shows that their coefficient of variation is only 0.06, which means that the representation of test results is quite adequate. By contrast, for constant $G_c$ the errors are much larger (Bažant and Cedolin, 1983b).

It is useful to realize the geometrical relationship of the R-curve to the family of the curves of equilibrium states (Equation (13.34)) for geometrically similar specimens of various sizes $d$. Introducing relative size $\lambda = d/d_a$ where $d_a$ is the maximum size of aggregate, the curves of $W'$ versus $c$ at various constant values of $\lambda$, defined by Equation (13.34), form a one-parameter family of curves characterized by the equation $F(c, W', \lambda) = 0$ where $F = bG_c(c) - W'(a_0 + c, \lambda)$. Differentiating this equation with respect to $c$, we get $(\partial F/\partial c) + (\partial F/W')W'' + (\partial F/\partial\lambda)(d\lambda/dc) = 0$, in which $\partial F/\partial c = bG_c'(c)$, $\partial F/\partial W' = -1$. Now the envelope of the family of the aforementioned curves is given by the condition $\partial F/\partial\lambda = 0$, and we see that this condition leads to the relation $bG_c'(c) - W'' = 0$, which is

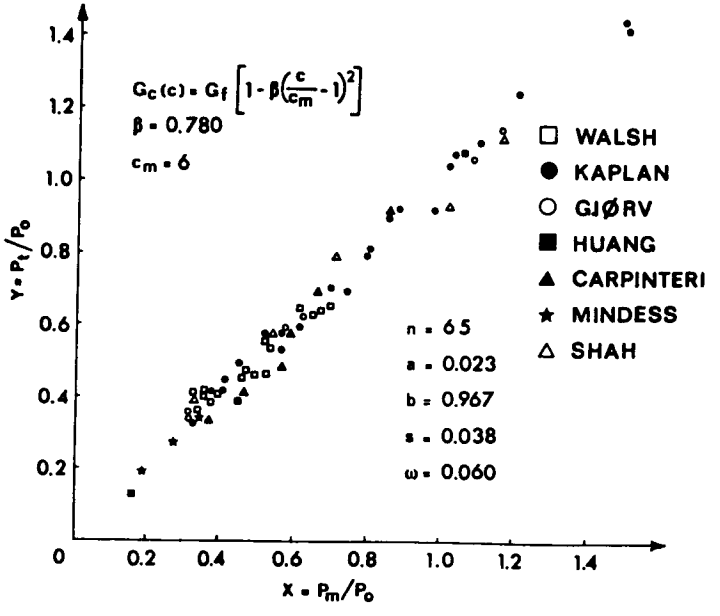


Figure 13.19 Statistical linear regression of measured failure loads versus theoretical ones (after Bažant and Cedolin, 1983b)

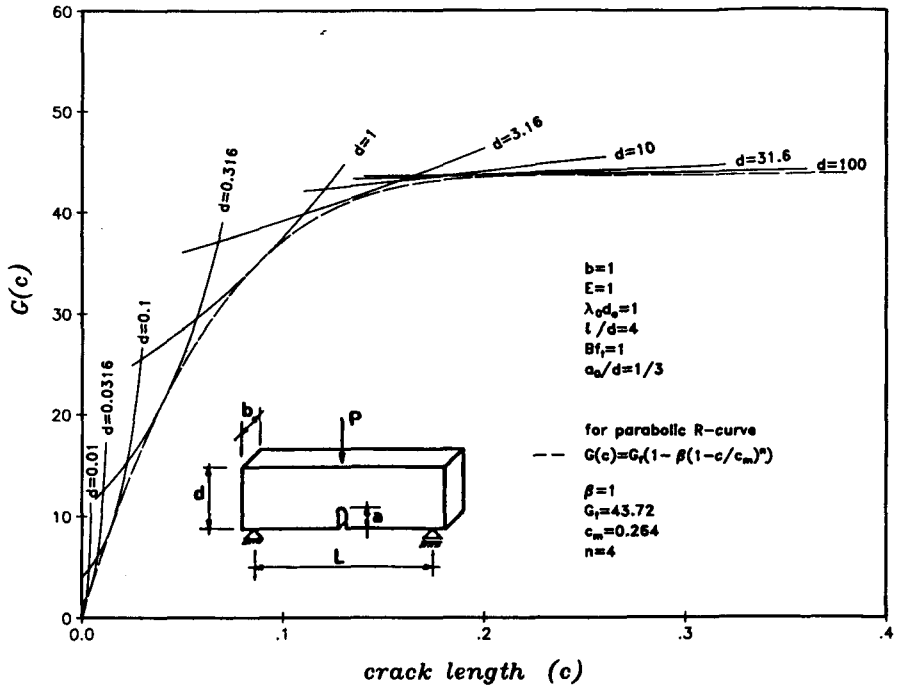


Figure 13.20 Determination of R-curve as an envelope of the curves of equilibrium states based on maximum load values for specimens of various sizes

found to be the same as Equation (13.35b) for the critical equilibrium state. Therefore, the curve of critical states may be geometrically obtained as the *envelope* of the curves of Equation (13.34) for various structure sizes; see Figure 13.20. We now show that this property permits a very simple determination of the R-curve from experimental data.

Assume that the curve $\sigma_N(\lambda)$, defined by Equation (13.16) which results from dimensional analysis, has been determined from experimental results. Thus, the failure loads (maximum loads or critical states) for various structure sizes $d$ are $P = bd\,\sigma_N(\lambda)$ in which $\lambda = d/d_a$, and substituting this into Equation (13.34), we obtain

$$\frac{1}{b}W' = \frac{d_a}{E_c}\lambda\sigma_N^2(\lambda)g(\alpha), \qquad \alpha = \frac{a_0 + c}{\lambda d_a} \tag{13.44}$$

in which $\sigma_N^2 = B^2 f_t'^2(1 + \lambda/\lambda_0)$ from Equation (13.16). Equation (13.44) defines a family of curves of $W'$ versus $c$ and various constant values of the relative size $\lambda$. This family of curves is illustrated in Figure 13.20 for the three-point bent specimens used by Walsh, as mentioned before. As is seen from Figure 13.20 it is very easy to obtain the envelope of these curves graphically. This envelope



represents the R-curve ($W'/b = G_c$) which exactly corresponds to the size effect according to Equation (13.16) based on dimensional analysis, for this type of specimen. Obviously, for another geometrical shape of specimen, a different R-curve is obtained in this manner. It appears, however, that the differences are not very significant in comparison with the typical scatter of experimental measurements.

To obtain the R-curve analytically, one needs to differentiate Equation (13.44) with regard to $\lambda$, which yields

$$\frac{2\lambda^2}{\sigma_N}\frac{d\sigma_N}{d\lambda} + \lambda - \frac{a_0 + c}{nd_a}\frac{g'(\alpha)}{g(\alpha)} = 0 \tag{13.45}$$

Equations (13.44) and (13.45) represent two algebraic equations for the R-curve, with $\lambda$ as a parameter. For some forms of function $g(\alpha)$, parameter $\lambda$ can be eliminated algebraically, yielding a single formula for the R-curve. However, this is not possible in general and a graphical construction of the envelope (Figure 13.20) is preferable.

It may be noted that the R-curve obtained graphically in Figure 13.20 can be quite closely approximated by a power curve. The approximation with an ellipse is worse.

The experimental determination of the R-curve just described is both simpler and more realistic than the existing methods. The existing methods utilize the relation $G_c = k_1 P^2 a/(E_c b^2 d^2)$, in which $k_1$ is a known coefficient for a given type of specimen. The values of $G_c$ are determined either on a single specimen from loads $P$ corresponding to various crack lengths $a$ or on a series of specimens from critical loads $P$ and the corresponding critical crack lengths $a$. In both cases, one needs to measure the crack length, which is an almost insurmountable obstacle in the case of concrete. First of all, the crack length is very difficult to define since the crack tip is blurred by a micro-cracking zone. Second, even if the crack length could be measured optically or otherwise, its usefulness is dubious because, as should be recalled, $a$ represents an equivalent crack length rather than some actual crack length. In view of these difficulties, it has been attempted to determine $a$ by measuring specimen compliance, either at unloading or at reloading. However, this is again of questionable relevance because at unloading or reloading the micro-cracks within the fracture process zone do not close and behave in a stiff manner, while for continued loading they have a much smaller stiffness. Therefore, the compliance measurements are likely to yield crack length values which are much too small.

All these shortcomings are avoided by the method proposed here. The scatter of measurements can be effectively removed by the use of Equation (13.16), which permits linear regression analysis in the plot of $\sigma_N^{-2}$ versus $\lambda$. This plot has the vertical axis intercept $(Bf_t')^{-2}$ and the slope $(Bf_t')^{-2}\lambda_0^{-1}$. After determining these parameters, the R-curve is then obtained as illustrated in Figure 13.20. Measurements of crack lengths are not needed at all. Determination of material

parameters entirely relies on maximum load data for geometrically similar specimens of various sizes. Such data are very easy to obtain, even in a small laboratory with the most rudimentary equipment.

## 13.7 CRACK SPACING AND CRACK SHEAR

For concrete structures, it is of importance to model not only isolated fractures but also systems of cracks. Of particular interest is the system of parallel equidistant cracks which forms under a uniform tensile loading of a panel reinforced by a mesh of bars, or in a beam with longitudinal reinforcement subjected to tension or bending. For the parallel crack system, it is necessary to determine the spacing of the cracks, after which the crack width can be estimated, and also the overall strain at which the cracks form. This problem has been traditionally analysed on the basis of strength criteria, coupled with the conditions of bond slip. However, the strength criteria govern only the initiation of micro-cracking, since they pertain to the peak point of the tensile stress–strain diagram. For a complete crack formation, strain-softening must reduce the stress to zero, which means that the full strain energy under the tensile stress–strain diagram must be dissipated. Therefore, complete crack formation should properly be calculated from energy fracture criteria. This approach has been taken in Bažant and Oh (1983), and simplified formulas for the crack spacing based on energy analysis were determined. Since the cracks are usually spaced rather closely compared to the maximum aggregate size, the energy balance conditions have been written for the sudden formation of the crack over its entire length. The formulas obtained from this fracture mechanics approach agreed reasonably well with the scant data on crack spacing and crack width available in the literature. Aside from energy balance, the evolution of crack spacing of a growing crack system is also governed by certain stability conditions; see Bažant, Ohtsubo and Aoh (1979).

Crack width is rather important for the shear transmission capability of cracks in concrete, which is essential for the load carrying capability of concrete structures. The shear response of cracks in concrete may be characterized by an incremental relation expressing the increments of the normal and shear stress transmitted across a crack as a function relative displacement (opening) and the tangential relative displacement (slip); see Bažant and Gambarova (1984).

## ACKNOWLEDGMENT

Partial financial support under AFOSR Grant No. 83–0009 to Northwestern University is gratefully appreciated. Mary Hill deserves thanks for her excellent secretarial assistance.



## REFERENCES

ASCE (1982) State-of-the-Art Report on *Finite Element Analysis of Reinforced Concrete*, prepared by a Task Committee chaired by A. Nilson, Am. Soc. of Civil Engrs., New York.

Batdorf, S. B., and Budiansky, B. (1949) 'A mathematical theory of plasticity based on the concept of slip', NACA TN 1871, April, 1949.

Barenblatt, G. I. (1959) 'The formation of equilibrium cracks during brittle fracture, general ideas and hypothesis. Axially-symmetric cracks', *Prikladnaya Matematika i Mekhanika*, **23**, 3, 434–444.

Bažant, Z. P. (1976) 'Instability, ductility and size effect in strain-softening concrete', *J. of the Engineering Mechanics Division, ASCE*, **102**, E2, 331–344.

Bažant, Z. P. (1982) 'Crack band model for fracture of geomaterials', *Proc., 4th Intern. Conf. on Numerical Methods in Geomechanics*, held in Edmonton, Alberta, Canada, June 1982 (Ed. Z. Eisenstein), Vol. 3 (invited lectures), 1137–1152.

Bažant, Z. P. (1983a) 'Size effect in brittle failure of concrete structures', *Report No. 83–2/665s*, Center for Concrete and Geomaterials, Northwestern University, Evanston, Illinois; also *Jour. of Engng. Mech. ASCE*, **110** (1984), 518–535.

Bažant, Z. P. (1983b) 'Imbricate continuum: variational formulation', *Report No. 83–11/428i*, Center for Concrete and Geomaterials, Northwestern University, Evanston, Illinois; also *J. of Eng. Mech. ASCE*, **110**, No. 10, Dec. 1984.

Bažant, Z. P. (1984) 'Mechanics of fracture and progressive cracking in concrete structures', in *Fracture Mechanics Applied to Concrete Structures* (Ed. G. C. Sih), Martinus Nijhoff Publishers, The Hague.

Bažant, Z. P., and Belytschko, T. B. (1983) 'Wave propagation in a strain-softening bar: exact solution', *Report No. 83–10/401w*, Center for Concrete and Geomaterials, Northwestern University, Evanston, Illinois; also *J. of Eng. Mech. ASCE*, in press.

Bažant, Z. P., and Cedolin, L. (1979) 'Blunt crack band propagation in finite element analysis', *Journal of the Engineering Mechanics Division, ASCE*, **105**, EM2, 297–315.

Bažant, Z. P., and Cedolin, L. (1980) 'Fracture mechanics of reinforced concrete', *Journal of the Engineering Mechanics Division, ASCE*, **106**, 1287–1306; with Discussion and Closure in **108**, 464–471 (1982).

Bažant, Z. P., and Cedolin, L. (1983a) 'Finite element modeling of crack band propagation', *Journal of Structual Engineering, ASCE*, **109**, ST2, 69–92.

Bažant, Z. P., and Cedolin, L. (1983b) 'Approximate linear analysis of concrete fracture by R-curves', *Report No. 83–7/679a*, Center for Concrete and Geomaterials, Technological Institute, Northwestern University, Evanston, Illinois; also *Jour. of Structural Engineering*, **110** (1984), 1336–1355.

Bažant, Z. P., and Gambarova, P. (1980) 'Rough cracks in reinforced concrete', *J. of the Struct. Div., Proc. ASCE*, **106**, 819–842; Discussion pp. 2579–2581.

Bažant, Z. P., and Gambarova, P. (1984) 'Crack shear in concrete: crack band microplane model', *Journal of Structural Engineering ASCE*, **110**, 2015–2035.

Bažant, Z. P., and Kim, J. K. (1984) 'Size effect in shear failure of longitudinally reinforced beams', *American Concrete Institute Journal*, **81**, 456–468.

Bažant, Z. P., and Oh, B. H. (1982) 'Rock fracture via stress–strain relations', Concrete and Geomaterials, *Report No. 82–11/665r*, Northwestern University, Evanston, Illinois; also *Jour. of Engng. Mechanics ASCE*, **110** (1984), 1015–1035.

Bažant, Z. P., and Oh, B. H. (1983a) 'Crack band theory for fracture of concrete', *Materials and Structures (RILEM, Paris)*, **16**, 155–177.

Bažant, Z. P., and Oh, B. H. (1983b) in 'Microplane model for fracture analysis of concrete

structures', *Proc. Symp. on the 'Interaction of Nonnuclear Munitions with Structures'*, US Air Force Academy, Colorado Springs, May 1983, pp. 49–55.
Bažant, Z. P., and Oh, B. H. (1983c) 'Model of weak planes for progressive fracture of concrete and rock', *Report No.* 83–2/448*m*, Center for Concrete and Geomaterials, Northwestern University, Evanston, Illinois.
Bažant, Z. P., and Oh, B. H. (1983) 'Spacing of cracks in reinforced concrete', *J. of Engng. Mech. ASCE*, Vol. 109, Sept. 1983, pp. 2266–2212.
Bažant, Z. P., and Panula, L. (1978) 'Statistical stability effects in concrete failure', *J. of the Engineering Mechanics Division, ASCE*, **104**, EM5, 1195–1212.
Bažant, Z. P., and Pfeiffer, P. (in preparation) 'Finite element crack band analysis'.
Bažant, Z. P., Ohtsubo, H., and Aoh, K. (1979) 'Stability and post-critical growth of a system of cooling or shrinkage cracks', *International Journal of Fracture*, **15**, 5, 443–456.
Bažant, Z. P., Pfeiffer, P., and Marchertas, A. H. (1983a) 'Blunt crack band propagation in finite element analysis for concrete structures', Preprints 7th Int. Conf. on Structural Mechanics in Reactor Technology, Chicago, Aug. 1983.
Bažant, Z. P., Chang, T. P., and Belytschko, T. B. (1983b) 'Continuum theory for strain softening', *Report No.* 83–11/428*c*, Center for Concrete and Geomaterials, Northwestern University, Evanston, Illinois; also *Journal of Engineering Mechanics ASCE*, **110**, in press.
Bhal, N. S. (1968) 'Über den Einfluss der Balkenhöhe auf Schubtragfähihkeit von einfeldrigen Stahlbetonbalken mit und ohne Schubbewehrung, Dissertation, Universität Stuttgärt.
Broek, D. (1974) *Elementary Engineering Fracture Mechanics*, Noordhoff International Publishing, Leyden, Netherlands.
Brown, J. H. (1972) 'Measuring the fracture toughness of cement paste and mortar', *Magazine of Concrete Research*, **24**, 81, 185–196.
Burt, W. J., and Dougill, J. W. (1977) 'Progressive failure in a model of heterogeneous medium', *J. of the Engng. Mechanics Division, Proc. ASCE*, **103**, EM3, 365–376.
Carpinteri, A. (1980) 'Static and energetic fracture parameters for rocks and concretes', Report, Istituto di Scienza delle Costruzioni-Ingegneria, University of Bologna, Italy.
Carpinteri, A. (1981) 'Experimental determination of fracture toughness parameters $K_{IC}$ and $J_{IC}$ for aggregative materials', *Advances in Fracture Research', Proc., 5th International Conference on Fracture*, Cannes, France, 1981 (Ed. D. François), Vol. 4, pp. 1491–1498.
Cedolin, L., and Bažant, Z. P. (1980) 'Effect of finite element choice in blunt crack band analysis', *Computer Methods in Applied Mechanics and Engineering*, **24**, 3, 305–316.
Cedolin, L., Dei Poli, S., and Iori, L. (1983a) 'Experimental determination of the fracture process zone in concrete', *Cement and Concrete Research*, **13** (to appear).
Cedolin, L., Dei Poli, S., and Iori, L. (1983b) 'Experimental determination of the stress–strain curve and fracture zone for concrete in tension', *Proc., Int. Conf. on Constitutive Laws for Engineering Materials* (Ed. C. Desai), University of Arizona, Tucson, January.
Dugdale, D. S. (1960) 'Yielding of steel sheets containing slits', *J. Mech. Phys. Solids*, **8**, 100–108.
Entov, V. M., and Yagust, V. I. (1975) 'Experimental investigation of laws governing quasi-static development of macrocracks in concrete', *Mechanics of Solids* (translation from Russian), **10**, 4, 87–95.
Eringen, A. C., and Ari, N. (1983) 'Nonlocal stress field at Griffith crack', *Cryst. Latt. Def. and Amorph. Mat.*, **10**, 33–38.
Eringen, A. C., and Edelen, D. G. B. (1972) 'On nonlocal elasticity', *Int. J. Engng. Science*, **10**, 233–248.



Evans, R. H., and Marathe, M. S. (1968) 'Microcracking and stress–strain curves for concrete in tension', *Materials and Structures* (*RILEM, Paris*), 1, Jan.–Feb., pp. 61–64.
Gjørv, O. E., Sørensen, S. I., and Arnesen, A. (1977) 'Notch sensitivity and fracture toughness of concrete', *Cement and Concrete Research*, **7**, 333–344.
Hadamard, J. (1903) *Leçons sur la propagation des ondes*, Hermann, Paris, Chapter VI.
Heilmann, H. G., Hilsdorf, H. H., and Finsterwalder, K. (1969) 'Festigkeit und Verformung von Beton unter Zugspanungen', *Deutscher Ausschuss für Stahlbeton*, Heft 203, W. Ernst & Sohn, West Berlin.
Hillerborg, A., Modéer, M., and Petersson, P. E. (1976) 'Analysis of crack formation and crack growth in concrete by means of fracture mechanics and finite elements', *Cement and Concrete Research*, **6**, 773–782.
Huang, C. M. J. (1981) 'Finite element and experimental studies of stress intensity factors for concrete beams', Thesis submitted in partial fulfillment of the requirements for the degree of Doctor of Philosophy, Kansas State University, Kansas.
Ingraffea, A. (1984) in *Fracture Mechanics Applied to Concrete Structures* (Ed. G. C. Sih and A. Carpinteri), Martinus Nijhoff Publishers, The Hague.
Irwin, G. R., Report of a Special Committee (1960) 'Fracture testing of high strength sheet materials', *ASTM Bulletin*, January 1960, p. 29 (also G. R. Irwin, 'Fracture testing of high strength sheet materials under conditions appropriate for stress analysis', *Report No.* 5486, Naval Research Laboratory, July 1960).
Kani, G. N. J. (1966) 'Basic facts concerning shear failure', Part I and Part II, *J. of ACI*, **63**, 6, 675–692.
Kaplan, M. F. (1961) 'Crack propagation and the fracture of concrete', *American Concrete Institute Journal*, **58**, 11.
Kesler, C. E., Naus, D. J., and Lott, J. L. (1971) 'Fracture mechanics—Its applicability to concrete', *International conference on the Mechanical Behaviour of Materials*, Kyoto, August 1971.
Kfouri, A. P., and Miller, K. J. (1974) 'Stress displacement, line integral and closure energy determinations of crack tip stress intensity factors', *Int. Journal of Pres. Ves. and Piping*, **2**, 3, 179–191.
Kfouri, A. P., and Rice, J. R. (1977) 'Elastic/plastic separation energy rate for crack advance in finite growth steps', in *Fracture* 1977 (Proc. of the 4th Intern. Conf. on Fracture, held in Waterloo, Ontario, June 1977) (Ed. D. M. R. Taplin), University of Waterloo Press, Vol. 1, pp. 43–59.
Knauss, W. C., 'On the steady propagation of a crack in a viscoelastic sheet; experiments and analysis', in *The Deformation in Fracture of High Polymers* (Ed. H. H. Kausch), Plenum Press, pp. 501–541.
Knott, J. F. (1973) '*Fundamentals of Fracture Mechanics*, Butterworths, London.
Krafft, J. M., Sullivan, A. M., Boyle, R. W. (1961) 'Effect of dimensions on fast fracture instability of notched sheets', *Cranfield Symposium*, 1961, Vol. I, pp. 8–28.
Kröner, E. (1967) 'Elasticity theory of materials with long-range cohesive forces', *Int. J. Solids Structures*, **3**, 731–742.
Kröner, E. (1968) 'Interrelations between various branches of continuum mechanics', *Mechanics of Generalized Continua* (Ed. E. Kröner), Springer-Verlag, pp. 330–340.
Krumhansl, J. A. (1968) 'Some considerations of the relation between solid state physics and generalized continuum mechanics', *Mechanics of Generalized Continua* (Ed. E. Kröner), Springer-Verlag, pp. 298–311.
Kunin, I. A. (1968) 'The theory of elastic media with microstructure and the theory of dislocations', *Mechanics of Generalized Continua* (Ed. E. Kröner), Springer-Verlag, pp. 321–328.

Leonhardt, F., and Walther, R. (1961/1962/1963) 'Beiträge zur Behandlung der Schubprobleme im Stahlbetonbau', *Beton-u Stahlbetonbau*, **56**, 12 (1961); **57**, 2, 3, 6, 7, 8, (1962); **58**, 8, 9 (1963).

Levin, V. M. (1971) 'The relation between mathematical expectation of stress and strain tensors in elastic microheterogeneous media', *Prikladnaya Matematika i Mekhanika*, **35**, 694–701 (in Russian).

Marchertas, A. H., Kulak, R. F., and Pan. Y. C. (1982) 'Performance of blunt crack approach within a general purpose code', in *Nonlinear Numerical Analysis of Reinforced Concrete* (Ed. L. E. Schwer), Am. Soc. of Mech. Engrs., New York (presented at ASME Winter Annual Meeting, Phoenix, November 1982), pp. 107–123.

Mindess, S. (1983) 'The application of fracture mechanics to cement and concrete: a historical review', in State-of-the-Art Report of RILEM Technical Committee 50-FMC on *Fracture Mechanics of Concrete*', (Ed. F. H. Wittmann), Elsevier, Netherlands.

Mindess, S., and Diamond, S. (1980) 'A preliminary SEM study of crack propagation in mortar', *Cement and Concrete Research*, **10**, 509–519.

Mindess, S., Lawrence, F. V., and Kesler, C. E. (1977) 'The J-integral as a fracture criterion for fiber reinforced concrete', *Cement and Concrete Research*, **7**, 731–742.

Naus, D. J. (1971) 'Applicability of linear-elastic fracture mechanics to Portland cement concretes', Thesis submitted in partial fulfillment of the requirements for the degree of Doctor of Philosophy, University of Illinois at Urbana-Champaign.

Pan, Y. C., and Marchertas, A. H. (1983) Private communication, May 1983, at Argonne National Laboratory, Argonne, Illinois.

Pan, Y. C., Marchertas, A. H., and Kennedy, J. M. (1983) 'Finite element of blunt crack band propagation: a modified J-integral approach', Preprints *7th Intern. Conf. on Structural Mechanics in Reactor Technology*, Paper H, Chicago, August 1983.

Parker, A. P. (1981) *The Mechanics of Fracture and Fatigue*, E. & F. N. Spon, Ltd.—Methuen, London.

Petersson, P. E. (1980) 'Fracture energy of concrete: method of determination', *Cement and Concrete Research*, **10**, 78–89; and 'Fracture energy of concrete: practical performance and experimental results', *Cement and Concrete Research*, **10**, 91–101.

Petersson, P. C. (1981) 'Crack growth and development of fracture zones in plain concrete and similar materials', Doctoral Dissertation, Lund Institute of Technology, Lund, Sweden.

Rashid, Y. R. (1968) 'Analysis of prestressed concrete pressure vessels', *Nuclear Engng. and Design*, **7**, 4, 334–344.

Reinhardt, H. W., and Cornelissen, H. A. W. (1984), 'Post-Peak Cyclic Behavior of Concrete in Uniaxial Tensile and Alternating Tensile and Compressive Loading', *Cement and Concrete Research*, **14**, 263–270.

Rice, J. R. (1976) 'The localization of plastic deformation', in *Theoretical and Applied Mechanics*, Preprints, IUTAM Congress held in Delft, 1976 (ed. W. T. Koiter), North-Holland, Amsterdam, pp. 207–220.

Rudnicki, J. W., and Rice, J. R. (1975) 'Conditions for the localization of deformation in pressure-sensitive dilatant materials', *J. of Mech. and Physics of Solids*, **23**, 371–394.

Rüsch, M., Haugli, F. R., and Mayer, M. (1962) 'Schubversuche an Stahlbeton Rechteckbalken mit Gleichmässig Verteilter Belastung', *Deutscher Ausschuss für Stahlbeton*, Heft 145, W. Ernst und Sohn, West Berlin.

Rüsh, H., and Hilsdorf, H. (1963) 'Deformation characteristics of concrete under axial tension', *Voruntersuchungen*, Bericht Nr. 44, Munich, May.

Shah, S. P. (1984) in *Fracture Mechanics Applied to Concrete Structures* (Ed. G. C. Sih and A. Carpinteri), Martinus Nijhoff Publishers, The Hague.

Shah, S. P., and McGarry, F. J. (1971) 'Griffith fracture criterion and concrete', *Journal of the Engineering Mechanics Division, ASCE*, **97**, EM6, 1663–1676.



Sok, C., Baron, J., and François, D. (1979) 'Mécanique de la rupture appliquée au beton hydraulique', *Cement and Concrete Research*, **9**.

Swamy, R. N., and Qureshi, S. A. (1971) 'Strength, cracking and deformation similitude in reinforced T-beams under bending and shear', Part I and II, *J. of Am. Concrete Inst.*, **68**, 3, 187–195.

Swartz, S. E., Hu, K. K., Fartash, M., and Huang, C. M. J. (1981) 'Stress intensity factors for plain concrete in bending—prenotched versus precracked beams', Report, Department of Civil Engineering, Kansas State University, Kansas.

Tada, H., Paris, P. C., and Irwin, G. R. (1973) *The Stress Analysis of Cracks Handbook*, Del Research Corp., Hellertown, Pa.

Taylor, G. I. (1938) 'Plastic strain in metals', *J. Inst. Metals*, **63**, 307–324.

Taylor, H. P. J. (1972) 'The shear strength of large beams', *J. of the Structural Division, ASCE*, **98**, 2473–2490.

Thomas, T. Y. (1961) *Plastic Flow and Fracture in Solids*, Academic Press.

Walraven, J. C. (1978) 'The influence of depth on the shear strength of lightweight concrete beams without shear reinforcement', *Stevin Laboratory Report No.* 5–78–4, Delft University of Technology.

Walsh, P. F. (1972) 'Fracture of plain concrete', *The Indian Concrete Journal*, **46**, 11, 469, 470, and 476.

Wecharatana, M., and Shah, S. P. (1980) 'Resistance to crack growth in Portland Cement Composites', Report, Department of Material Engineering, University of Illinois at Chicago, Chicago, Illinois.

Witmann, F. H. (Ed.) (1983) *Fracture Mechanics of Concrete*, Elsevier, Netherlands.

Wnuk, M. P. (1974) 'Quasi-static extension of a tensile crack contained in viscoelastic plastic solid', *Journal of Applied Mechanics, ASME*, **41**, 1, 234–248.